Sigma), NANOG (1:100, ReproCELL), OCT3/4 (1:200, Santa Cruz Biotechnology), SSEA-4 (1:200, Millipore), TRA-1-60 (1:200, Millipore), TH (1:100, Millipore), α-synuclein (1:500, Invitrogen), pα-synuclein (1:1000, Wako), cleaved-Caspase3 (1:500, Cell Signaling) and ComplexIII (C-III)-core I (1:200, Invitrogen). Cells were washed with PBS after incubation with the primary antibody, followed by incubation with an Alexa Fluor 488-, Alexa Fluor 555-, or Alexa Fluor 647-conjugated secondary antibody (1:500, Invitrogen). Images were obtained using Apotome (Zeiss) or LSM-710 confocal (Zeiss) microscopes.

PCR amplification of genomic DNA

Genomic DNA was purified from HDFs and iPSCs using a DNeasy kit (Qiagen). The PCR conditions used have been previously described [2,42].

Reverse transcription (RT)-PCR

RNA isolation and reverse transcription (RT)-PCR were performed as previously described [44]. The amount of cDNA was normalized to *β-actin* mRNA. Real-time RT-PCR was performed on a ABI PRISM Sequence detection System 7900HT (Applied BioSystems) using SYBR premix ExTaq (Takara). Primers for the detection of Oct4, the transgenes *Oct4-tg, Sox2-tg, Klf4-tg* and *c-Myc-tg,* and MAO-A, and -B have been previously described [10,15].

Teratoma assay

To assess teratoma formation, iPSCs were injected into the testis of 8-week-old NOD/SCID mice (OYG International) as previously described [14]. Eight weeks after transplantation, tumors were dissected and fixed with 4% PFA in PBS. Paraffin-embedded tissue was sectioned and stained with H&E. Images were obtained using a BZ-9000 (Keyence) microscope.

CGH array

Genomic DNA was restricted, labeled, and purified using the Agilent Oligo CGH Microarray Kit (Agilent Technologies) according to the manufacturer's protocol. Labeled genomic DNA was processed for hybridization on a 4x 180K microarray (Agilent Technologies). Processing was performed as instructed by the manufacturer. The genomic analysis was performed using Agilent Genomic Workbench ver. 6.0 software (Agilent Technologies).

Metabolism assays

Reduced GSH levels were measured according to the kit manufacturer's protocol (GSH-Glo Glutathione Assay; Promega). Chymotrypsin-like proteasome activity was measured using a Cell-Based Proteasome-Glo Assay according to the manufacturer's instructions (Promega). Briefly, neural cells (1.0×10^4) derived from neurospheres were seeded in triplicate into a white 96-well plate (Nunc). Prepared reagent (100 μl) was added to each well. After incubation for 10 min at RT, luminescence intensity was recorded. ROS levels were determined by measuring DCFH-DA fluorescence (Invitrogen). Briefly, neurons were incubated with 5 μM DCFH-DA and Hoechst (1:2000) for 30 min at 37°C, after which they were washed with PBS and then incubated in differentiation media. Fluorescence was measured by an In Cell Analyzer 2000 system (GE Healthcare Biosciences).

Protein analysis

Differentiated neurons were harvested in MAPK lysis buffer containing proteinase inhibitor, and protein concentrations were measured by BCA assay (Thermo Scientific). Samples were diluted to yield equivalent protein concentrations and then 4 μg was denatured by the addition of 4X sample buffer (Invitrogen) supplemented with β-mercaptoethanol followed by boiling. Samples (7 μl/lane) were loaded onto a 4–20% SDS-polyacrylamide gradient gel. Membranes were incubated in blocking solution with the indicated primary antibodies at 4°C overnight. Immunoreactive proteins were detected with horseradish peroxidase (HRP)-conjugated secondary antibodies and then visualized by chemiluminescence (Pierce, Rockford, IL, USA) according to the manufacturer's instructions. Quantification of band intensities was performed using an RAS4000 system. The primary antibodies used were anti-NQO1 (1:1000, Abcam), anti-NRF2 (1:1000, Santa Cruz Biotechnology) and β-actin (1:5000, Cell Signaling).

CCCP and Baf A_1 treatments

Neurons were cultured with 30 μM CCCP (Sigma-Aldrich) or DMSO, with or without 5 μM Baf A_1 (Sigma-Aldrich), for 48 h. The cells were then fixed and stained for βIII-tubulin and C-III Core I, and counterstained with Hoechst. To quantify the IMM area of the neurons, the cytoplasmic area was extracted as shown in Figure 3C. The C-III Core I-positive signals within the extracted area were then converted to gray-scale and digitized. The IMM area was quantified from the digitized values using Image J software.

Tetramethylrhodamine ethyl ester (TMRE) staining

iPSC-derived neurons were incubated with 1nM TMRE (Invitrogen) for 15 min at 37°C and then observed under an Olympus IX81 microscope.

Electron microscopy

Cells were fixed with 2% glutaraldehyde/2% PFA in 0.1 M phosphate buffer (PB) (pH7.2), post-fixed with 1% OsO4 in 0.1 M PB (pH 7.2), blocked and stained with a 2% aqueous solution of uranyl acetate, dehydrated with a graded series of ethanol, and then embedded in Epon 812 (TAAB). Coverslips were detached and the embedded samples were placed under a stereomicroscope to identify the cells of

interest. Ultrathin sections were cut with a Leica UC6 or UC7 ultramicrotome (Leica Microsystems) and then stained with uranyl acetate and lead citrate. Samples were observed with a Hitachi H7100 or HT7700 electron microscope.

Morphometry

Morphometric analysis was used to measure the volume density of mitochondria in the neuronal perikarya as previously described [45]. Briefly, electron micrographs of neurons (n = 20, 23, 41, and 44 for control A (B7), control B (WD39), PA9 and PB2, respectively) were obtained at a magnification of ×7000. After enlarging to three times the original magnification, point-counting was carried out to determine the volume density using a double-lattice test system with 1.5 cm spacing. Mitochondria were classified as normal, abnormal, or undetermined. The abnormal mitochondria were defined as those with irregularly arranged cristae, or with a high electron-dense matrix. The volume density (Vv) of each type of mitochondrion was expressed as percent volume according to the following formula: Vv = (Pi/Pt) × 100 (%), where Pi is the number of points falling on each mitochondrial structure and Pt is the number of points falling on the neuronal perikarya.

Immunohistochemical analysis of autopsied brain tissue

The ethical committee of the Kitasato University School of Medicine and Juntendo University School of Medicine reviewed and approved the protocol for analysis of autopsied brain tissue. Patients and control subjects were informed of the study and gave written informed consent. Brain tissue from patient PA was obtained following her death at age 72; brain tissue from the father of patient PB was obtained when he died at age 70 [46]. Tissue was fixed with 10% formalin and then embedded in paraffin. Midbrain sections (6 μm thick) were cut, deparaffinized with xylene, and then rehydrated in ethanol. After being boiled and treated with H_2O_2, sections were subjected to immunofluorescence staining with antibodies to the following proteins: α-synuclein (1:500, Invitrogen), pα-synuclein (1:1000, Wako), and TH (1:1000, Calbiochem). After washing with PBS, sections were incubated with a biotinylated secondary antibody (1:500; Vector Laboratories Inc.) at RT for 1 hr followed by incubation with an avidin-biotin peroxidase complex (Vector Laboratories Inc.) for 1 hr. Immunoreactive proteins were visualized using 3,3-diaminobenzidine (DAB; Wako Pure Chemical Industries) and nuclear fast red staining. For immunofluorescence, FITC-conjugated and Cy3-conjugated secondary antibodies (1:500; Jackson Immunoresearch Laboratories) were used. Images were obtained using a BIOREVO (Keyence) and a confocal laser-scanning LSM710 (Zeiss) microscope.

Statistical analysis

Values represent the mean ± SEM. The Mann–Whitney *U*-test was used to evaluate differences between groups. A P value of < 0.05 was considered significant.

Additional files

Additional file 1: Genetic studies of family. (A) An arrow indicates PA patient. (B) An arrow indicates PB patient. Filled circles and squares, women and men with PARK2 mutation; Open circles and squares, normal women and men; Diamond shapes, family members whose DNA samples were not analyzed. Symbols with lines through them represent the deceased.

Additional file 2: Characterization of control and PARK2 iPSCs. (A) Control A (YA9), Control B (WD39), PA (PA9), and PB (PB2) iPSCs expressed the pluripotency markers SSEA4 (red) and TRA1-60 (green). Scale bar, 100 μm. (B) iPSCs established from patients PA (PA1, PA22) and PB (PB1, PB18, and PB20) were positive for the pluripotency markers Nanog (red), Oct4 (green), SSEA4 (red), and TRA1-60 (green). Scale bars: phase images, 200 μm; immunofluorescence images, 100 μm. (C) Levels of endogenous *Oct4* mRNA in the generated iPSCs were similar to those in KhES1 cells, a human embryonic stem cell (hESC) line [42]. Expression levels were normalized to that of KhES1 (set as 1). (D) Cont A (YA9), Cont B (WD39), PA (PA1, 9 and 22), and PB (PB1, 2, 18 and 20) iPSCs gave rise to teratomas with all three germ layers, confirming pluripotency. Scale bar, 100 μm. (E) Silencing of transgenes in control and PARK2 iPSC clones. Expression levels were normalized to the positive control of fibroblasts in cultures assayed 6 days after retroviral infection (= 100). Cont A, Control A; Cont B, Control B.

Additional file 3: Confirmation of *parkin* deletions and genomic stability of PARK2 iPSCs using comparative genomic hybridization (CGH) microarray analysis. (A) Exons 2–4 were deleted in the PA9 and PA22 iPSC lines. Exons 6 and 7 were deleted in the PB2, 18, and 20 iPSC lines. (B) Copy number profiles of whole chromosomes in PARK2 iPSCs assessed by CGH microarray analysis revealed that no genomic aberrations were introduced during the process of establishing PARK2 iPSCs.

Additional file 4: Expression level of MAO-A and -B showed no difference among Control and PARK2 iPSC-derived neurons. (A,B) qRT-PCR measurement of MAO-A and -B transcripts in PARK2 (PA (1, 9 and 22) and PB (1, 2 and 20)) iPSC-derived neurons showed no difference compared to those in Cont A (B7 and YA9). ContA; Control A, ContB; Control B.

Additional file 5: Healthy mitochondria in PARK2 fibroblasts and iPSCs. (A, B) Electron micrographs of fibroblasts (upper panels) and iPSCs (lower panels) from Control (Cont A and Cont B) and PARK2 patients (PA and PB). Mitochondria in the fibroblasts and iPSCs from both groups showed long, cylindrical profiles with well-organized cristae, and the electron density of the matrix was relatively low (asterisks). Scale bar, 0.25 μm. Cont A, Control A; Cont B, Control B. (C) Fibroblasts were treated with 30μM CCCP or DMSO for 48 h, followed by staining for CIII corel (magenta) to label the internal mitochondrial membrane (IMM) and counterstaining with Hoechst (Ho, blue). Mitochondrial size decreased after CCCP treatment in both Control (Cont A and Cont B) and PARK2 (PA and PB) fibroblasts. Scale bar, 20 μm. (D) iPSCs were treated with 30 μM CCCP or DMSO for 48 h and then stained for CIII corel (magenta) to label IMM, Oct4 (blue) to label iPSCs, and Hoechst (Ho, white). Mitochondrial size in Control (Cont A (B7), Cont B (WD39)), and PARK2 (PA9 and PB2) iPSCs decreased after CCCP treatment. Scale bar, 20 μm (E) CCCP/DMSO ratios in Control (Cont A (B7, YA9), Cont B (WD39)), and PARK2 (PA9 and 22 and PB2 and 20) iPSCs (Mann Whitney *U*-test). Data represent the mean and SEM ($n > 3$ for each group).

Additional file 6: Mitochondrial membrane potential after CCCP treatment in control and PARK2 iPSC-derived neurons. (A) iPSC-derived neurons were treated with 30 μM CCCP or DMSO for 48 h, after which they were stained for the mitochondrial membrane potential marker, TMRE. The intensity of TMRE (yellow) was clearly reduced in

control (Cont A (B7), Cont B (WD39)), and PARK2 (PA9 and PB2) iPSC-derived neurons. Scale bar, 50 μm.

Additional file 7: Confirmation of *parkin* deletions carried by the father of patient PB. (A) Deletion of exons 6 and 7 was confirmed in blood samples from PB and the father of PB by PCR.

Additional file 8: α-Synuclein signals are not seen in PARK2 iPSCs. (A) Quantitative genomic PCR analysis for SNCA exons 1 and 4 demonstrated a normal copy number in PARK2 (PA1, 9 and 22, and PB1, 2, 18 and 20) iPSCs. The copy number was the same as that observed for Cont A (B7 and YA9) and Cont B (WD39). The *SNCA* gene copy number was normalized to β-globin *(HBB)* and β2-microglobulin *(B2MG)*. (B) iPSCs were stained for α-synuclein (red), Oct4 (green; to label iPSCs) and Hoechst (blue). No α-synuclein signals were observed in Cont A (B7 and YA9), Cont B (WD39), or PARK2 (PA9 and 22, PB2 and 20) iPSCs. Scale bar, 50 μm.

Competing interests
The authors declare that they have no competing interests.

Authors' contributions
YI, YO, WA, and HO conceived and designed the experiments. YI performed most of the experiments, analyzed data, and wrote the manuscript. YO, and HO edited the manuscript. YO developed the quality control system, neural differentiation method for the iPSCs and performed CGH microarray data analysis. WA generated the WD39 iPSCs. NK, KH, MS and AN performed western blotting analysis. TN performed some parts of *in vitro* culture assay. SS, MF, YM, HM and NH examined and recruited PARK2 patients. TK, MO, and MA performed biopsies and established the skin fibroblasts. AH, TS, TH and MS performed preliminary experiments for the metabolome analysis. TY, DI, AK and NS provided cent8-1 iPSCs. YI and NM designed the CCCP treatment experiment. MK and YU performed the electron microscopic analysis. HH, MT, HM and NH performed the histopathological studies of the postmortem brain of PA. All authors read and approved the final manuscript.

Acknowledgments
We would like to thank S. Yamanaka (CiRA) for the 201B7 iPSCs; N. Nakatsuji (Kyoto University) for the KhES cells; N. Izawa, S. Banno, Y. Matsuzaki, M. Fujiwara, Y. Nagahata, N. Hirose (Keio University), C. Kishi (Tokyo Medical and Dental University), M. Ogino, S. Miyakawa, (Kitasato University) and G. Takata (GE Healthcare Biosciences) for technical assistance and suggestions. This work was supported by the Project for the Realization of Regenerative Medicine and Support for the Core Institutes for iPS cell research from the Japanese Ministry of Education, Culture, Sports, Science and Technology (MEXT) to H.O., Exploratory Research for Advanced Technology (ERATO), Suematsu Gas Biology Project from Japan Science and Technology Agency (JST) to M.S., a Grant-in-Aid from the Japan Society for the Promotion of Science (JSPS) to W.A. and Y.O., the Keio Kanrinmaru Project and a Grant-in-Aid for Scientific Research on Innovative Areas to Y.O., a Grant-in-Aid for Scientific Research on Innovative Areas (Comprehensive Brain Science Network) from the MEXT to Y. O. and Y. I., a Grant-in-Aid for Encouragement of Young Medical Scientists from Keio University and the Japan Society for the Promotion of Science Fellows to Y.I., and a Grant-in-Aid for the Global COE Program at Keio University.

Author details
[1]Department of Physiology, Keio University School of Medicine, 35 Shinanomachi, Shinjuku-ku, Tokyo 160-8582, Japan. [2]Kanrinmaru Project, Keio University School of Medicine, Tokyo, Japan. [3]Department of Cell Biology and Neuroscience, Juntendo University Graduate School of Medicine, Tokyo, Japan. [4]Department of Neurology, Kitasato University School of Medicine, Kanagawa, Japan. [5]Department of Dermatology, Keio University School of Medicine, Tokyo, Japan. [6]Department of Neurology, Juntendo University School of Medicine, Tokyo, Japan. [7]Research Institute for Diseases of Old Age, Graduate School of Medicine, Juntendo University, Tokyo, Japan. [8]Institute for Advanced Biosciences, Keio University, Yamagata, Japan. [9]Department of Biochemistry, Keio University School of Medicine, Tokyo, Japan. [10]Department of Neurology, Keio University School of Medicine, Tokyo, Japan. [11]Advanced Science Research Laboratories, Pharmaceutical Research Division, Takeda Pharmaceutical Company Limited, Kanagawa, Japan. [12]Department of Neuro-Regenerative Medicine, Kitasato University School of Medicine, Kanagawa, Japan. [13]Department of Physiology and Cell Biology, Tokyo Medical and Dental University, Tokyo, Japan. [14]Department of Neurology, Osaka University Graduate School of Medicine, Osaka, Japan.

Received: 19 September 2012 Accepted: 2 October 2012
Published: 6 October 2012

References
1. Farrer MJ: **Genetics of Parkinson disease: paradigm shifts and future prospects.** *Nature reviews* 2006, **7**:306–318.
2. Kitada T, Asakawa S, Hattori N, Matsumine H, Yamamura Y, Minoshima S, Yokochi M, Mizuno Y, Shimizu N: **Mutations in the parkin gene cause autosomal recessive juvenile parkinsonism.** *Nature* 1998, **392**:605–608.
3. Shimura H, Hattori N, Kubo S, Mizuno Y, Asakawa S, Minoshima S, Shimizu N, Iwai K, Chiba T, Tanaka K, Suzuki T: **Familial Parkinson disease gene product, parkin, is a ubiquitin-protein ligase.** *Nat Genet* 2000, **25**:302–305.
4. Whitworth AJ, Pallanck LJ: **The PINK1/Parkin pathway: a mitochondrial quality control system?** *J Bioenerg Biomembr* 2009, **41**:499–503.
5. Youle RJ, Narendra DP: **Mechanisms of mitophagy.** *Nat Rev Mol Cell Biol* 2011, **12**:9–14.
6. Goldberg MS, Fleming SM, Palacino JJ, Cepeda C, Lam HA, Bhatnagar A, Meloni EG, Wu N, Ackerson LC, Klapstein GJ, *et al*: **Parkin-deficient mice exhibit nigrostriatal deficits but not loss of dopaminergic neurons.** *J Biol Chem* 2003, **278**:43628–43635.
7. Palacino JJ, Sagi D, Goldberg MS, Krauss S, Motz C, Wacker M, Klose J, Shen J: **Mitochondrial dysfunction and oxidative damage in parkin-deficient mice.** *J Biol Chem* 2004, **279**:18614–18622.
8. Perez FA, Palmiter RD: **Parkin-deficient mice are not a robust model of parkinsonism.** *Proc Natl Acad Sci USA* 2005, **102**:2174–2179.
9. Sato S, Chiba T, Nishiyama S, Kakiuchi T, Tsukada H, Hatano T, Fukuda T, Yasoshima Y, Kai N, Kobayashi K, *et al*: **Decline of striatal dopamine release in parkin-deficient mice shown by ex vivo autoradiography.** *J Neurosci Res* 2006, **84**:1350–1357.
10. Jiang H, Ren Y, Yuen EY, Zhong P, Ghaedi M, Hu Z, Azabdaftari G, Nakaso K, Yan Z, Feng J: **Parkin controls dopamine utilization in human midbrain dopaminergic neurons derived from induced pluripotent stem cells.** *Nat Commun* 2012, **3**:668.
11. Mattis VB, Svendsen CN: **Induced pluripotent stem cells: a new revolution for clinical neurology?** *Lancet Neurol* 2011, **10**:383–394.
12. Farrer M, Chan P, Chen R, Tan L, Lincoln S, Hernandez D, Forno L, Gwinn-Hardy K, Petrucelli L, Hussey J, *et al*: **Lewy bodies and parkinsonism in families with parkin mutations.** *Ann Neurol* 2001, **50**:293–300.
13. Savitt JM, Dawson VL, Dawson TM: **Diagnosis and treatment of Parkinson disease: molecules to medicine.** *J Clin Invest* 2006, **116**:1744–1754.
14. Ohta S, Imaizumi Y, Okada Y, Akamatsu W, Kuwahara R, Ohyama M, Amagai M, Matsuzaki Y, Yamanaka S, Okano H, Kawakami Y: **Generation of human melanocytes from induced pluripotent stem cells.** *PLoS One* 2011, **6**:e16182.
15. Takahashi K, Tanabe K, Ohnuki M, Narita M, Ichisaka T, Tomoda K, Yamanaka S: **Induction of pluripotent stem cells from adult human fibroblasts by defined factors.** *Cell* 2007, **131**:861–872.
16. Matigian N, Abrahamsen G, Sutharsan R, Cook AL, Vitale AM, Nouwens A, Bellette B, An J, Anderson M, Beckhouse AG, *et al*: **Disease-specific, neurosphere-derived cells as models for brain disorders.** *Dis Model Mech* 2010, **3**:785–798.
17. Nguyen HN, Byers B, Cord B, Shcheglovitov A, Byrne J, Gujar P, Kee K, Schule B, Dolmetsch RE, Langston W, *et al*: **LRRK2 mutant iPSC-derived DA neurons demonstrate increased susceptibility to oxidative stress.** *Cell Stem Cell* 2011, **8**:267–280.
18. Sies H: **Glutathione and its role in cellular functions.** *Free Radic Biol Med* 1999, **27**:916–921.
19. Williamson TP, Johnson DA, Johnson JA: **Activation of the Nrf2-ARE pathway by siRNA knockdown of Keap1 reduces oxidative stress and provides partial protection from MPTP-mediated neurotoxicity.** *Neurotoxicology* 2012, **33**:272–279.
20. Ramsey CP, Glass CA, Montgomery MB, Lindl KA, Ritson GP, Chia LA, Hamilton RL, Chu CT, Jordan-Sciutto KL: **Expression of Nrf2 in neurodegenerative diseases.** *J Neuropathol Exp Neurol* 2007, **66**:75–85.
21. Tufekci KU, Civi Bayin E, Genc S, Genc K: **The Nrf2/ARE Pathway: a promising target to counteract mitochondrial dysfunction in parkinson's disease.** *Parkinsons Dis* 2011, **2011**:314082.

22. Fukae J, Mizuno Y, Hattori N: **Mitochondrial dysfunction in Parkinson's disease.** *Mitochondrion* 2007, **7**:58–62.
23. Schapira AH: **Mitochondrial dysfunction in neurodegenerative disorders.** *Biochim Biophys Acta* 1998, **1366**:225–233.
24. Greene JC, Whitworth AJ, Kuo I, Andrews LA, Feany MB, Pallanck LJ: **Mitochondrial pathology and apoptotic muscle degeneration in Drosophila parkin mutants.** *Proc Natl Acad Sci USA* 2003, **100**:4078–4083.
25. Mortiboys H, Thomas KJ, Koopman WJ, Klaffke S, Abou-Sleiman P, Olpin S, Wood NW, Willems PH, Smeitink JA, Cookson MR, Bandmann O: **Mitochondrial function and morphology are impaired in parkin-mutant fibroblasts.** *Ann Neurol* 2008, **64**:555–565.
26. Matsuda N, Sato S, Shiba K, Okatsu K, Saisho K, Gautier CA, Sou YS, Saiki S, Kawajiri S, Sato F, *et al*: **PINK1 stabilized by mitochondrial depolarization recruits Parkin to damaged mitochondria and activates latent Parkin for mitophagy.** *J Cell Biol* 2010, **189**:211–221.
27. Narendra D, Tanaka A, Suen DF, Youle RJ: **Parkin is recruited selectively to impaired mitochondria and promotes their autophagy.** *J Cell Biol* 2008, **183**:795–803.
28. Tanaka A: **Parkin-mediated selective mitochondrial autophagy, mitophagy: Parkin purges damaged organelles from the vital mitochondrial network.** *FEBS Lett* 2010, **584**:1386–1392.
29. Yoshii SR, Kishi C, Ishihara N, Mizushima N: **Parkin mediates proteasome-dependent protein degradation and rupture of the outer mitochondrial membrane.** *J Biol Chem* 2011, **286**:19630–19640.
30. Seibler P, Graziotto J, Jeong H, Simunovic F, Klein C, Krainc D: **Mitochondrial Parkin recruitment is impaired in neurons derived from mutant PINK1 induced pluripotent stem cells.** *J Neurosci* 2011, **31**:5970–5976.
31. Shults CW: **Lewy bodies.** *Proc Natl Acad Sci USA* 2006, **103**:1661–1668.
32. Pramstaller PP, Schlossmacher MG, Jacques TS, Scaravilli F, Eskelson C, Pepivani I, Hedrich K, Adel S, Gonzales-McNeal M, Hilker R, *et al*: **Lewy body Parkinson's disease in a large pedigree with 77 Parkin mutation carriers.** *Ann Neurol* 2005, **58**:411–422.
33. Sasaki S, Shirata A, Yamane K, Iwata M: **Parkin-positive autosomal recessive juvenile Parkinsonism with alpha-synuclein-positive inclusions.** *Neurology* 2004, **63**:678–682.
34. Schlossmacher MG, Frosch MP, Gai WP, Medina M, Sharma N, Forno L, Ochiishi T, Shimura H, Sharon R, Hattori N, *et al*: **Parkin localizes to the Lewy bodies of Parkinson disease and dementia with Lewy bodies.** *Am J Pathol* 2002, **160**:1655–1667.
35. Chung KK, Zhang Y, Lim KL, Tanaka Y, Huang H, Gao J, Ross CA, Dawson VL, Dawson TM: **Parkin ubiquitinates the alpha-synuclein-interacting protein, synphilin-1: implications for Lewy-body formation in Parkinson disease.** *Nat Med* 2001, **7**:1144–1150.
36. Petrucelli L, O'Farrell C, Lockhart PJ, Baptista M, Kehoe K, Vink L, Choi P, Wolozin B, Farrer M, Hardy J, Cookson MR: **Parkin protects against the toxicity associated with mutant alpha-synuclein: proteasome dysfunction selectively affects catecholaminergic neurons.** *Neuron* 2002, **36**:1007–1019.
37. Shimura H, Schlossmacher MG, Hattori N, Frosch MP, Trockenbacher A, Schneider R, Mizuno Y, Kosik KS, Selkoe DJ: **Ubiquitination of a new form of alpha-synuclein by parkin from human brain: implications for Parkinson's disease.** *Science (New York, NY)* 2001, **293**:263–269.
38. Yagi T, Kosakai A, Ito D, Okada Y, Akamatsu W, Nihei Y, Nabetani A, Ishikawa F, Arai Y, Hirose N, *et al*: **Establishment of induced pluripotent stem cells from centenarians for neurodegenerative disease research.** *PLoS One* 2012, **7**:e41572.
39. Hargus G, Cooper O, Deleidi M, Levy A, Lee K, Marlow E, Yow A, Soldner F, Hockemeyer D, Hallett PJ, *et al*: **Differentiated Parkinson patient-derived induced pluripotent stem cells grow in the adult rodent brain and reduce motor asymmetry in Parkinsonian rats.** *Proc Natl Acad Sci USA* 2010, **107**:15921–15926.
40. Park IH, Arora N, Huo H, Maherali N, Ahfeldt T, Shimamura A, Lensch MW, Cowan C, Hochedlinger K, Daley GQ: **Disease-Specific Induced Pluripotent Stem Cells.** *Cell* 2008, .
41. Soldner F, Hockemeyer D, Beard C, Gao Q, Bell GW, Cook EG, Hargus G, Blak A, Cooper O, Mitalipova M, *et al*: **Parkinson's disease patient-derived induced pluripotent stem cells free of viral reprogramming factors.** *Cell* 2009, **136**:964–977.
42. Devine MJ, Ryten M, Vodicka P, Thomson AJ, Burdon T, Houlden H, Cavaleri F, Nagano M, Drummond NJ, Taanman JW, *et al*: **Parkinson's disease induced pluripotent stem cells with triplication of the alpha-synuclein locus.** *Nat Commun* 2011, **2**:440.
43. Suemori H, Yasuchika K, Hasegawa K, Fujioka T, Tsuneyoshi N, Nakatsuji N: **Efficient establishment of human embryonic stem cell lines and long-term maintenance with stable karyotype by enzymatic bulk passage.** *Biochem Biophys Res Commun* 2006, **345**:926–932.
44. Okada Y, Matsumoto A, Shimazaki T, Enoki R, Koizumi A, Ishii S, Itoyama Y, Sobue G, Okano H: **Spatiotemporal recapitulation of central nervous system development by murine embryonic stem cell-derived neural stem/progenitor cells.** *Stem cells (Dayton, Ohio)* 2008, **26**:3086–3098.
45. Koike M, Shibata M, Waguri S, Yoshimura K, Tanida I, Kominami E, Gotow T, Peters C, von Figura K, Mizushima N, *et al*: **Participation of autophagy in storage of lysosomes in neurons from mouse models of neuronal ceroid-lipofuscinoses (Batten disease).** *Am J Pathol* 2005, **167**:1713–1728.
46. Mitsui J, Takahashi Y, Goto J, Tomiyama H, Ishikawa S, Yoshino H, Minami N, Smith DI, Lesage S, Aburatani H, *et al*: **Mechanisms of genomic instabilities underlying two common fragile-site-associated loci, PARK2 and DMD, in germ cell and cancer cell lines.** *Am J Hum Genet* 2010, **87**:75–89.

doi:10.1186/1756-6606-5-35
Cite this article as: Imaizumi *et al.*: Mitochondrial dysfunction associated with increased oxidative stress and α-synuclein accumulation in PARK2 iPSC-derived neurons and postmortem brain tissue. *Molecular Brain* 2012 5:35.

Lewy Body Pathology in a Patient With a Homozygous *Parkin* Deletion

Saori Miyakawa, MD,[1]* Mieko Ogino, MD, PhD,[1] Sayaka Funabe, MD,[2,3] Akiko Uchino, MD,[1] Yasushi Shimo, MD, PhD,[2] Nobutaka Hattori, MD, PhD,[2] Masaaki Ichinoe, MD, PhD,[4] Tetuo Mikami, MD, PhD,[4] Makoto Saegusa, MD, PhD,[4] Kazutoshi Nishiyama, MD, PhD,[1] Hideo Mori, MD, PhD,[2] Yoshikuni Mizuno, MD, PhD,[5] Shigeo Murayama, MD, PhD[3] and Hideki Mochizuki, MD, PhD[6]

[1]*Department of Neurology, Kitasato University School of Medicine, Kanagawa, Japan;* [2]*Department of Neurology, Juntendo University School of Medicine, Tokyo, Japan;* [3]*Department of Neuropathology, Tokyo Metropolitan Institute of Gerontology, Tokyo, Japan;* [4]*Department of Pathology, Kitasato University School of Medicine, Kanagawa, Japan;* [5]*Department of Neuroregenerative Medicine, Kitasato University School of Medicine, Kanagawa, Japan;* [6]*Department of Neurology, Osaka University School of Medicine, Osaka, Japan.*

ABSTRACT

Background: We report neuropathologic findings in a patient with homozygous deletions of exons 2 to 4 of *parkin*.

Results: Although the absence of Lewy bodies has been considered a neuropathologic characteristic of *parkin* mutation, here we report a pathologic finding with the presence of Lewy bodies.

Methods: The patient was a 72-year-old woman with onset of the disease at age 61. Her autopsy revealed marked decrease in melanized neurons in the substantia nigra and the locus coeruleus. Lewy bodies were found in the substantia nigra, the locus coeruleus, the dorsal motor nucleus of the vagus, the basal nucleus of Meynert, the amygdaloid nucleus, and the sympathetic nerve bundles in the myocardium.

Conclusions: Only 3 previous case reports described Lewy body formation in patients carrying *parkin* mutations. The distribution of Lewy bodies in our patient appeared to be reminiscent of sporadic Parkinson's disease. © 2013 *Movement* Disorder Society

Key Words: PARK2; Lewy body; α-synuclein; parkin; neuropathology

Parkinsonism associated with *parkin* mutations (PARK2) is characterized by early onset (age < 40 years), slow progression, good response to levodopa, sleep benefit, levodopa-induced motor fluctuations, and dyskinesias.[1–5] Selective neuronal degeneration in the pigmented neurons of the substantia nigra (SN) without Lewy body formation is considered a pathologic characteristic of PARK2-linked Parkinson's disease (PD)[6–11]; however, Lewy body–positive cases have also been reported.[12–14] We had a chance to see an autopsied case of a PARK2 patient who had numerous Lewy bodies in the brain.

Case Report

The patient was a 72-year-old woman. She noted onset of difficulty in walking in her left leg at age 61. At age 64, difficulty in walking spread to her right leg with start hesitation. She was seen at Juntendo University Hospital on December 13, 2001. She showed tremor in her left hand, mild rigidity, bradykinesia, gait disturbance, and postural instability. Her parents were first cousins. Her mother was said to have PD, but the details were not clear. Her father did not have PD.

Her brain MRI was unremarkable. Cardiac MIBG scintigraphy at age 66 was normal (heart-to-mediastinum uptake ratio was 2.27 in the early phase and 2.14 in the delayed phase; normal value for the institute, >1.45). Genetic analysis revealed homozygous deletions of exons 2–4 of *parkin*.

She was at Yahr stage I to II with cabergoline. At age 67, levodopa/carbidopa was started because of postural instability. She had no orthostatic hypotension or dementia. She began to have wearing-off and dyskinesia at age 68. She received bilateral STN-DBS at age 71 with improvement in her motor fluctuation. At age 72, she was admitted to our hospital because of severe pneumonia. Shortly after admission, her clinical status deteriorated, and she died of respiratory failure. Autopsy was performed 2 hours after death.

*Correspondence to: Dr. Saori Miyakawa, Department of Neurology, Kitasato University, School of Medicine, 1-15-1 Kitasato, Minami-ku, Sagamihara, Kanagawa, 252-0374, Japan; saomiya@med.kitasato-u.ac.jp

Relevant conflicts of interest/financial disclosures: Yoshikuni Mizuno is a professor of a department that was donated by Boehlinger-Ingelheim, Japan, Inc., and Medotronics, Japan, Inc.

Full financial disclosures and author roles may be found in the online version of this article.

Received: 13 August 2012; **Revised:** 25 November 2012; **Accepted:** 29 November 2012
Published online 11 February 2013 in Wiley Online Library (wileyonlinelibrary.com).
DOI: 10.1002/mds.25346

Neuropathologic Findings

The brain samples were embedded in paraffin, and sections 4 μm thick were made. They were stained with hematoxylin-eosin (HE), Klüver-Barrera, and Gallyas-Braak and immunostained with the following antibodies: antiphosphorylated α-synuclein (psyn #64, Dako, Kyoto, Japan), antiphosphorylated tau (AT8; Innogenetics, Temse, Belgium), and anti–amyloid-beta protein (11-28; IBL, Fujioka, Japan). The anterior walls of the left ventricles of the hearts of this patient, a patient with sporadic PD, and a control patient were stained with HE and immunostained with psyn #64, antityrosine hydroxylase (TH; Calbiochem, Darmstadt, Germany), and antiphosphorylated neurofilament (SMI31; Sternberger Immunochemicals, Bethesda, MD). Brains of the 3 patients with PD and dementia (PDD) were also stained for α-synuclein pathology for comparison.

The weight of the brain was 1260 g with no atrophy. The serial coronal sections of the brain and horizontal sections of the brain stem showed severe loss of pigmentation in the SN (Fig. 1a) and locus coeruleus (LC; Fig. 1b). Microscopically, the numbers of melanin-containing neurons were decreased in the SN (Fig. 1c) and LC. Lewy bodies were seen in the SN (Fig. 1c) and LC. Immunostaining with psyn #64 showed Lewy bodies and Lewy neuritis in the remaining neurons of the SN, LC (Fig. 1d), dorsal motor nucleus of the vagus (Fig. 1e), amygdaloid nucleus, basal nucleus of Meynert (nbM; Fig. 1f), striatum, and anterior cingulate cortex. Semiquantitative observation of Lewy-related pathology in 3 sporadic PD patients based on the scoring system of the Third Report of the DLB Consortium[15] revealed 3 (severe) in the SN and nbM in all 3 patients, and 3.7 ± 0.58 (4 [very severe], 4, and 3) in the amygdaloid nucleus (central), although in our patient, it was 3 in the SN, nbM, and amygdaloid nucleus (central). From the distribution of Lewy bodies, her brain corresponded to stage IV of Braak's classification.[16] Tau-positive inclusions were observed only in the entorhinal cortex. β-Amyloid plaques were absent.

Lewy bodies were also found in the adrenal medulla (Fig. 1g). The nerve fibers in the epicardium were shown to contain eosinophilic inclusions with HE staining, which were recognized by immunostaining with psyn #64 (Fig. 1h). Immunostaining for TH of the nerve fibers in the epicardium showed intense staining in the control patient, no immunostaining in the patient with sporadic PD, and intermediate staining in this patient. Immunostaining with phosphorylated neurofilament in the nerve fibers of the epicardium was the same intensity as the staining with TH immunostaining, indicating intermediate degeneration of the cardiac sympathetic nerve bundles.

Discussion

We have reported the pathology of a patient with homozygous deletions of exons 2–4 of *parkin* who had Lewy bodies in many areas of the brain. Until now, 3 cases of PARK2 with Lewy bodies have been reported in the literature (Table 1).[12–14] The case reported by Farrer et al was a man who had onset of the disease at age 41 and died at age 52.[12] He had compound heterozygous mutations of *parkin* (R275W at exon 7 and 40-base-pair deletion in exon 3). Loss of pigmented neurons and Lewy bodies were seen in the SN and LC. Immunostaining for α-synuclein revealed no Lewy bodies in other areas of the brain, except for a few Lewy bodies in the nbM and the amygdala-parahippocampal region and the occasional Lewy neurites in the dorsal motor nucleus of the vagus. Farrer et al stated that their case did not differ in any respect from that seen in mild to moderate idiopathic PD. The case reported by Sasaki et al was a woman who had onset of the disease at age 33 and died at age 70.[13] She had homozygous deletion of exon 3 in *parkin*. There was moderate loss of pigmented neurons in the SN and LC. Lewy bodies were not observed in the SN or the LC. Inclusion bodies resembling Lewy bodies but more basophilic were noted in the neuropil of the pedunculopontine nucleus. The case reported by Pramstaller et al was a man who had onset of the disease at age 49 and died at age 73.[14] Marked loss of neurons was found in the SN and LC. A small number of Lewy bodies were seen in the SN and LC. They could detect truncated Parkin protein in the SN of this patient. The presence of truncated Parkin may be a reason for the presence of Lewy bodies in our case. We confirmed the absence of full-length *parkin* in our case; however, the presence of truncated Parkin cannot be excluded completely.

Thus, the case reported by Farrer et al[12] is similar to our case, and the case reported by Parmstaller et al[14] has some resemblance, even though the number of Lewy bodies was smaller. In our patient, Lewy bodies were detected in many areas of the brain. This distribution of Lewy bodies may well be seen in sporadic PD. Until now 9 cases of autopsied PARK2 patients have been reported including ours,[7–14] of which 4 cases including ours had Lewy bodies.[12–14]

Cardiac uptake of ^{123}I-MIBG scintigraphy was normal in our case 5 years after onset when the patient was in stage III of Hoehn and Yahr. Pathological examination showed relatively preserved sympathetic nerve fibers in the epicardium compared with patients with sporadic PD.[17] But Lewy body formation was found in the epicardial nerve fibers. According to the literature, cardiac TH-positive fibers show marked degeneration in sporadic PD with α-synuclein deposition,[17] whereas TH-positive fibers were retained in PARK2.[18] In our patient, TH-positive fibers and epicardial axonal fibers

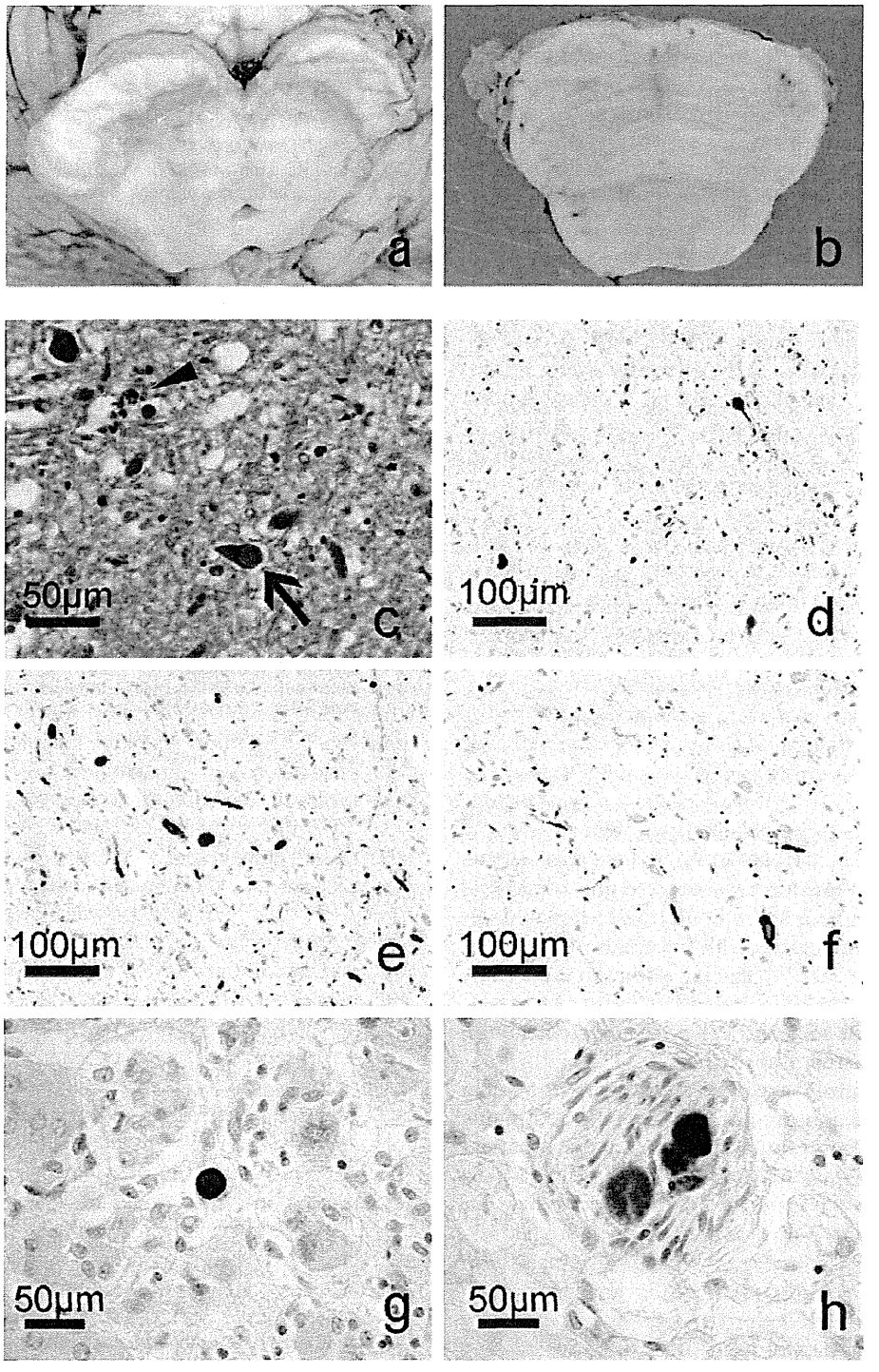

FIG. 1. Neuropathologic findings of the patient. The substantia nigra shows marked depigmentation in the macroscopic view (**a**). HE staining of the substantia nigra shows a Lewy body (arrow) in the remaining neuron (**c**), severe loss of pigmented neurons, and melanophagia (arrowhead). The locus coeruleus cannot be identified because of severe depigmentation in the macroscopic view (**b**). Immunostaining for α-synuclein shows a Lewy body in the remaining neurons and Lewy neuritis in the LC (**d**). Immunostaining for α-synuclein in the dorsal motor nucleus of the vagus (**e**), and the nbM (**f**) shows Lewy bodies and Lewy neuritis. The adrenal medulla also shows Lewy bodies by α-synuclein immunostaining (**g**). Immunostaining for α-synuclein of the nerve fibers in the epicardium shows Lewy bodies (**h**).

TABLE 1. Summary of Lewy body–positive and –negative cases of PARK2

	Sex	Age at onset	Age at death	Mutation	LB distribution
Lewy body–positive cases of PARK2					
Farrer et al, 2001	M	41	52	R275W, del 40 bp in Exon3	Transitional
Sasaki et al, 2004	F	33	70	Homozygous delExon3	Pedunculopontine
Pramistaller et al, 2005	M	49	73	delExon7, del1072T	Brain stem
Our patient	F	61	72	Homozygous delExon2–4	Transitional
Lewy body–negative cases of PARK2					
Yamamura et al, 1998	F	20	52	delExon3, delExon3	No LB
Mori et al, 1998	M	24	62	Homozygous delExon4	No LB
Hayashi et al, 2000	M	32	70	Homozygous delExon4	No LB
van de Warrenburg et al, 2001	M	18	75	Lys211Asn, delExon3	No LB
Gouider-Khouja et al, 2003	M	34	47	Homozygous dlbp101–102 in Exon2	No LB

did not show marked degeneration, despite the presence of α-synuclein aggregates in the cardiac sympathetic nerve fibers. The findings of cardiac sympathetic fibers were not typical of sporadic PD.

Then, why do some PARK2 patients have Lewy bodies and others do not? There seems to be no clear relation to the type of mutation. Among the 4 cases with Lewy bodies, 2 had compound heterozygous mutations[12,14] and 2 had homozygous mutations.[13] Homozygous deletions were found in 4 of 5 autopsy cases of Lewy body–negative patients,[7–9,11] and compound heterozygous mutations were in 1 patient.[10] The case reported by Yamamura et al in 1998 was reported to have homozygous deletions of exon 3.[6,19] In the case reported by Farrer et al,[12] expressed truncated Parkin protein was found in the lymphoblasts. Also, truncated Parkin protein was detected in the patient reported by Pramstaller et al.[14] Parkin protein could not be detected in the patient (without Lewy bodies) reported by Mori et al.[8,20] Parkin colocalizes with α-synuclein aggregates in Lewy bodies of PD.[21] Older age of onset may well be a reason for the positivity of Lewy bodies. However, the coexistence of sporadic PD process together with *parkin* mutation cannot be excluded.

In conclusion, we have reported a patient with a homozygous deletion of *parkin* who showed many Lewy bodies in the brain. We believe that this patient started with a Parkin-deficient brain followed by sporadic PD changes; however, further studies are necessary to explore this question. ■

References

1. Yamamura Y, Sobue I, Ando K, et al. Paralysis agitans of early onset with marked diurnal fluctuation of symptoms. Neurology 1973;23:239–244.
2. Ishikawa A, Tsuji S. Clinical analysis of 17 patients in 12 Japanese families with autosomal-recessive type juvenile parkinsonism. Neurology 1996;47:160–169.
3. Kitada T, Asakawa S, Hattori N, et al. Mutations in the parkin gene cause autosomal recessive juvenile parkinsonism. Nature 1998;392:605–608.
4. Lücking CB, Dürr A, Bonifati V, et al. Association between early-onset Parkinson's disease and mutations in the parkin gene. N Engl J Med 2000;342:1560–1567.
5. Periquet M, Latouche M, Lohmann E, et al. Parkin mutations are frequent in patients with isolated early-onset parkinsonism. Brain 2003;126:1271–1278.
6. Poulopoulos M, Levy OA, Alcalay RN. The neuropathology of genetic Parkinson's disease. Mov Disord 2012;27:831–842.
7. Yamamura Y, Kuzuhara S, Kondo K, et al. Clinical, pathologic and genetic studies on autosomal recessive early-onset parkinsonism with diurnal fluctuation. Parkinsonism Relat Disord 1998;4:65–72.
8. Mori H, Kondo T, Yokochi M, et al. Pathologic and biochemical studies of juvenile parkinsonism linked to chromosome 6q. Neurology 1998;51:890–892.
9. Hayashi S, Wakabayashi K, Ishikawa A, et al. An autopsy case of autosomal-recessive juvenile parkinsonism with a homozygous exon 4 deletion in the parkin gene. Mov Disord 2000;15:884–888.
10. van de Warrenburg BP, Lammens M, Lücking CB, et al. Clinical and pathologic abnormalities in a family with parkinsonism and parkin gene mutations. Neurology 2001;56:555–557.
11. Gouider-Khouja N, Larnaout A, Amouri R et al. Autosomal recessive parkinsonism linked to parkin gene in a Tunisian family. Clinical, genetic and pathological study. Parkinsonism Relat Disord 2003;9:247–251.
12. Farrer M, Chan P, Chen R, et al. Lewy bodies and parkinsonism in families with parkin mutations. Ann Neurol 2001;50:293–300.
13. Sasaki S, Shirata A, Yamane K, et al. Parkin-positive autosomal recessive juvenile parkinsonism with α-synuclein-positive inclusions. Neurology 2004;63:678–682.
14. Pramstaller PP, Schlossmacher MG, Jacques TS, et al. Lewy body Parkinson's disease in a large pedigree with 77 parkin mutation carriers. Ann Neurol 2005;58:411–22.
15. McKeith IG, Dickson DW, Lowe J, et al. Diagnosis and management of dementia with Lewy bodies. Third Report of the DLB Consortium. Neurology 2005;65:1863–1872.
16. Braak H, Tredici KD, Rub U, et al. Staging of brain pathology related to sporadic Parkinson's disease. Neurobiol Aging 2003;24:197–211.
17. Orimo S, Uchihara T, Nakamura A, et al. Axonal α-synuclein aggregates herald centripetal degeneration of cardiac sympathetic nerve in Parkinson's disease. Brain 2008;131:642–650.
18. Orimo S, Amino T, Yokochi M, et al. Preserved cardiac sympathetic nerve accounts for normal cardiac uptake of MIBG in PARK2. Mov Disord 2005;20:1350–1353.
19. Yamamura Y, Hattori N, Matsumine H, et al. Autosomal recessive early-onset parkinsonism with diurnal fluctuation: clinicopathologic characteristics and molecular genetic identification. Brain Dev 2000;22:S87–S91.
20. Shimura H, Hattori N, Kubo S, et al. Immunohistochemical and subcellular localization of Parkin: absence of protein in autosomal recessive juvenile parkinsonism patients. Ann Neurol 1999;45:668–672.
21. Schlossmacher MG, Frosch MP, Gai WP, et al. Parkin localizes to the Lewy bodies of Parkinson disease and dementia with Lewy bodies. Am J Pathol 2002;160:1655–1667.

nature COMMUNICATIONS

ARTICLE

Received 17 Sep 2012 | Accepted 20 Dec 2012 | Published 29 Jan 2013

DOI: 10.1038/ncomms2417

Heat shock factor-1 influences pathological lesion distribution of polyglutamine-induced neurodegeneration

Naohide Kondo[1], Masahisa Katsuno[1], Hiroaki Adachi[1], Makoto Minamiyama[1], Hideki Doi[1], Shinjiro Matsumoto[1], Yu Miyazaki[1], Madoka Iida[1], Genki Tohnai[1], Hideaki Nakatsuji[1], Shinsuke Ishigaki[1], Yusuke Fujioka[1], Hirohisa Watanabe[1], Fumiaki Tanaka[1], Akira Nakai[2] & Gen Sobue[1]

A crucial feature of adult-onset neurodegenerative diseases is accumulation of abnormal protein in specific brain regions, although the mechanism underlying this pathological selectivity remains unclear. Heat shock factor-1 is a transcriptional regulator of heat shock proteins, molecular chaperones that abrogate neurodegeneration by refolding and solubilizing pathogenic proteins. Here we show that heat shock factor-1 expression levels are associated with the accumulation of pathogenic androgen receptor in spinal and bulbar muscular atrophy, a polyglutamine-induced neurodegenerative disease. In heterozygous *heat shock factor-1*-knockout spinal and bulbar muscular atrophy mice, abnormal androgen receptor accumulates in the cerebral visual cortex, liver and pituitary, which are not affected in their genetically unmodified counterparts. The depletion of *heat shock factor-1* also expands the distribution of pathogenic androgen receptor accumulation in other neuronal regions. Furthermore, lentiviral-mediated delivery of heat shock factor-1 into the brain of spinal and bulbar muscular atrophy mice topically suppresses the pathogenic androgen receptor accumulation and neuronal atrophy. These results suggest that heat shock factor-1 influences the pathological lesion selectivity in spinal and bulbar muscular atrophy.

[1] Department of Neurology, Nagoya University Graduate School of Medicine, Nagoya 466-8550, Japan. [2] Department of Biochemistry and Molecular Biology, Yamaguchi University School of Medicine, Ube 755-8505, Japan. Correspondence and requests for materials should be addressed to M.K. (email: ka2no@med.nagoya-u.ac.jp).

Heat shock proteins (Hsps), including Hsp70 and Hsp40, are stress-induced molecular chaperones that have important roles in maintaining correct folding, the assembly of newly synthesized proteins and the intracellular transport of proteins[1,2]. There are various lines of evidence indicating that Hsps abrogate neurodegeneration by refolding and solubilizing pathogenic proteins[3,4]. Particularly, Hsp70 facilitates the proteasomal degradation of abnormal proteins and thereby ameliorates neuronal damage in cellular and animal models of adult-onset neurodegenerative disorders, including Alzheimer's disease, amyotrophic lateral sclerosis and Huntington' disease (HD)[5–7] and other polyglutamine diseases caused by the expansion of a genomic CAG repeat[8–10]. Among several molecules that control the expression of Hsps, heat shock factor-1 (Hsf-1) is shown to strongly regulate the expression of Hsp70 by activating its promoter[11,12].

To develop effective treatments for neurodegenerative disorders, it is important to elucidate the molecular mechanism by which only specific cells are affected, despite the broad expression of the disease-causing mutant genes. The selectivity of the pathogenic lesions in neurodegenerative diseases may be influenced by several factors. For example, the length of the CAG triplet repeat in the causative gene influences the distribution of pathological lesions of spinocerebellar ataxia type 7 and dentatorubral pallidoluysian atrophy[13,14]. Given that the length of the polyglutamine tract increases the propensity of the protein to aggregate, the pathological lesion selectivity of spinocerebellar ataxia type 7 appears to be influenced by the biological properties of the causative protein[15]. Alternatively, the expression of molecules that interact with the disease-causing proteins, such as PQBP-1 and Rhes, is also associated with the distribution of selective neuronal cell loss in polyglutamine diseases[16,17]. Furthermore, transcriptional factors such as nuclear transcription factor Y subunit alpha (NF-YA) and p53 were shown to, at least partially, determine the vulnerability of cells to polyglutamine-expanded proteins by regulating the expression of Hsps in cellular models of HD[18,19].

The accumulation of polyglutamine-expanded proteins is detected histopathologically as diffuse nuclear staining or as intraneuronal inclusion bodies, the distribution of which corresponds to that of pathological involvement and symptomatic phenotypes[20,21]. The intranuclear accumulation of disease-causing misfolded proteins is thought to trigger neurodegeneration by various mechanisms such as transcriptional dysregulation, impairment of axonal transport and mitochondrial dysfunction[22–24]. This view is supported by animal studies showing that the prevention of pathogenic protein accumulation successfully rescues the phenotype in model mice of polyglutamine diseases[25–28].

Here, we investigated the role of Hsf-1 in pathogenic lesion selectivity in spinal and bulbar muscular atrophy (SBMA), an adult-onset motor neuron disease caused by the expansion of a CAG repeat in the gene coding androgen receptor (AR)[29–31]. This disease affects susceptible regions, such as spinal anterior horn, brainstem and pancreas, despite the ubiquitous expression of the causative protein[32]. In the present study, we found that the heterozygous knockout of *Hsf-1* in SBMA model mice led to the extended distribution of pathogenic AR accumulation in neuronal and non-neuronal tissues as well as exacerbated neuromuscular phenotype, whereas the lentiviral overexpression of HSF-1 locally precludes pathogenic AR accumulation and neuronal atrophy in the brain of the SBMA mice.

Results

Hsf-1 levels are associated with pathogenic AR accumulation. To examine whether the expression levels of Hsf-1 are associated with the distribution of pathogenic AR accumulation in SBMA, we performed immunohistochemistry on the central nervous system (CNS) of a transgenic SBMA mouse model carrying human AR with 97 CAGs (AR-97Q). In this model animal, the full-length human AR was expressed ubiquitously (Supplementary Fig. S1a). The results showed that low expression levels of Hsf-1 were associated with a high frequency of pathogenic AR accumulation (Fig. 1a,b). For example, the accumulation of pathogenic AR is frequently observed in spinal motor neurons that show weak immunoreactivity for Hsf-1. In contrast, neurons in the cerebral cortex and striatum, most of which are Hsf-1-positive, were rarely stained with 1C2, a specific antibody against the expanded polyglutamine tract. In the cerebellum of AR-97Q mice, there was a scarce accumulation of pathogenic AR in Purkinje cells, where Hsf-1 was expressed at a high level. Conversely, there were abundant 1C2-positive cells in the cerebellar granular cell layer, which showed scarce immunoreactivity for Hsf-1 (Fig. 1a). There was little difference in the expression pattern of Hsf-1 between AR-97Q and wild-type mice, except for the spinal anterior horn, where the nuclear expression of Hsf-1 was decreased in AR-97Q mice compared with wild-type mice (Fig. 1a). Quantitative analysis of the relationship between the expression levels of Hsf-1 and the frequency of 1C2-positive cells in various parts of the CNS confirmed that higher expression levels of Hsf-1 are associated with the reduced accumulation of pathogenic AR (Fig. 1b). This relationship, however, was not clearly observed for Nfya, p53, TATA box-binding protein (Tbp) or Sp1, which are other potential inducers of Hsp70 (Supplementary Fig. S1b,c). These findings led us to focus on Hsf-1 as a possible regulator of the pathogenic lesion selectivity, especially in the CNS, of the SBMA model mouse.

Previous studies showed that AR-97Q mice show pathogenic AR aggregation in non-neuronal tissues, such as the heart, lung, pancreas and skeletal muscle, in addition to the CNS[25]. To examine whether the expression levels of Hsf-1 are also associated with pathogenic AR accumulation outside the CNS, we performed immunohistochemistry using anti-Hsf-1 and 1C2 antibodies on non-neuronal tissues of the AR-97Q mice. The results demonstrated that a similar relationship as seen in CNS was observed in the pancreas, liver and testis. There was unequivocal pathogenic AR accumulation in the pancreas, where Hsf-1 is expressed at a low level (Supplementary Fig. S1d). In contrast, no visible pathogenic AR accumulation was observed in the liver or testis, where Hsf-1 is expressed at a relatively high level (Supplementary Fig. S1d).

We further verified this relationship in autopsied specimens from SBMA patients. 1C2-positive cells were frequently detected in spinal motor neurons and pancreatic islet cells, where HSF-1 is expressed at a low level, compared with control subjects. In contrast, there were no 1C2-stained cells in the neuronal and non-neuronal tissues in which HSF-1 was expressed at a high level (Supplementary Fig. S2a,b).

Taken together, these results indicate that high expression levels of Hsf-1 are associated with reduced pathogenic AR accumulation in neuronal and non-neuronal tissues of the SBMA mouse model and SBMA patients.

***Hsf-1* depletion expands distribution of AR accumulation.** To clarify whether low expression levels of Hsf-1 have a causative role in the accumulation of pathogenic AR *in vivo*, we depleted *Hsf-1* in AR-97Q mice by crossing them with heterozygous *Hsf-1*-knockout mice[33]. As *Hsf-1*-null AR-97Q (AR-97Q Tg/−, *Hsf-1* −/−) mice were not obtained, presumably owing to their early death during embryonic development, we performed immunohistochemistry on various tissues from wild-type

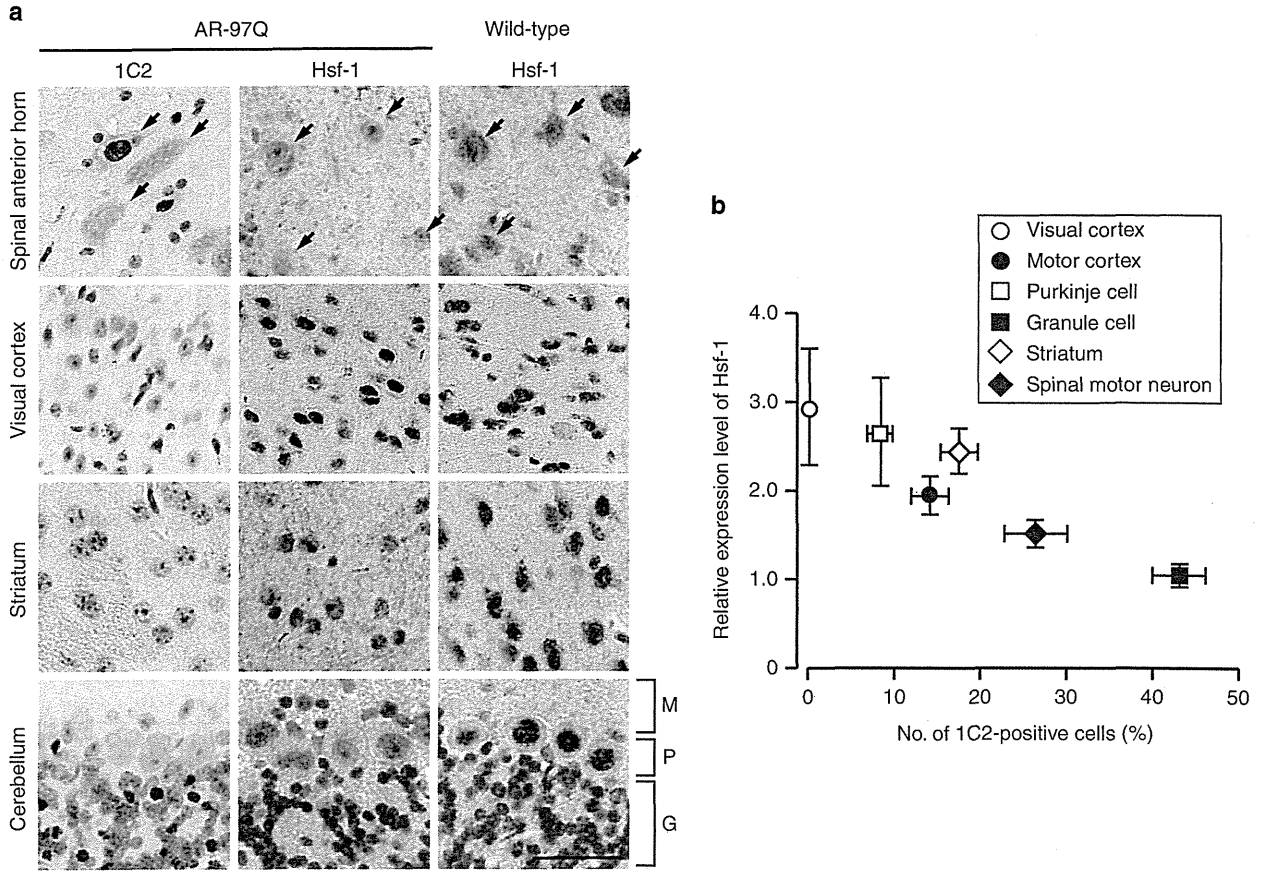

Figure 1 | Hsf-1 expression is associated with pathogenic AR accumulation. (**a**) Immunohistochemistry for Hsf-1 and expanded polyglutamine (1C2) in the spinal anterior horn, visual cortex, striatum and cerebellum from wild-type and AR-97Q mice (13 weeks old). Arrows indicate motor neurons within the spinal anterior horn. M, molecular layer; P, Purkinje cell layer; G, granular layer. (**b**) Quantification of the relationship between the nuclear immunoreactivity of Hsf-1 and the frequency of 1C2-positive cells in different parts of the CNS. More than 500 neurons in each part from three brains were analysed (**b**). Error bars indicate s.e.m. (**b**). Scale bars, 50 μm (**a**).

(AR-97Q −/−, *Hsf-1* +/+), AR-97Q (AR-97Q Tg/−, *Hsf-1* +/+) and heterozygous *Hsf-1*-knockout AR-97Q (AR-97Q Tg/−, *Hsf-1* +/−) mice, to examine whether Hsf-1 inactivation expands the distribution of pathogenic AR accumulation. The nuclear accumulation of pathogenic AR is not detected in the liver and pituitary gland of AR-97Q mice, even at an advanced stage (Supplementary Fig. S3). Surprisingly, we observed the nuclear accumulation of pathogenic AR in the liver of the heterozygous *Hsf-1*-knockout SBMA mice (Fig. 2a). Quantitative analysis showed that 1.40 ± 0.35% (1.0–2.1) of hepatocytes were positive for 1C2 in the *Hsf-1*-depleted AR-97Q mice, while no positive cells were observed in the AR-97Q mice ($n = 3$ per group). To confirm the effects of *Hsf-1* depletion on the metabolism of pathogenic AR, we performed immunoblotting of the liver samples using an anti-AR antibody. The results revealed that the expression level of AR monomer, which appears to be one of the toxic species of polyglutamine protein[34], was increased by the heterozygous knockout of *Hsf-1* in the liver of AR-97Q mice (Fig. 2b,c). Insoluble high-molecular-weight AR complexes, which may have a protective property, were not detected in the liver of either type of mice, presumably because of the relatively low expression levels of AR in this tissue.

To assess whether the accumulation of pathogenic AR due to *Hsf-1* depletion impairs liver function, we performed histology and blood tests on each mouse group. The serum levels of liver enzymes, such as aspartate aminotransferase and alanine aminotransferase, which are indicative of liver dysfunction, were significantly elevated in heterozygous *Hsf-1*-knockout AR-97Q mice compared with the genetically unmodified AR-97Q mice (Fig. 2d,e), while this was not the case for wild-type mice (Fig. 2f,g). Furthermore, immunohistochemistry demonstrated that the liver became atrophied in the heterozygous *Hsf-1*-knockout AR-97Q mice, but not in their wild-type counterparts (Fig. 2h–j). Similarly, pathogenic AR accumulation was also detected in the pituitary gland of the heterozygous *Hsf-1*-knockout SBMA mice (Fig. 2a). A total of 0.67 ± 0.17% (0.5–1.0) of the cells in the pituitary gland of the heterozygous *Hsf-1*-knockout AR-97Q mice exhibited the nuclear accumulation of pathogenic AR, although there were no 1C2-positive cells in the pituitary gland of genetically unmodified AR-97Q mice ($n = 3$ per group). These findings indicate that Hsf-1 prevents the accumulation of pathogenic AR in the liver and pituitary gland of AR-97Q mice.

A similar phenomenon was observed in certain parts of the CNS in AR-97Q mice. Interestingly, the accumulation of pathogenic AR was detected in the cerebral visual cortex of heterozygous *Hsf-1*-knockout SBMA mice (Fig. 3a), where the accumulation of pathogenic AR was not observed in the AR-97Q mice, even at an advanced stage (Supplementary Fig. S3). Furthermore, the heterozygous knockout of *Hsf-1* also augmented the accumulation of pathogenic AR in spinal motor neurons and Purkinje cells as well as the neurons of the striatum

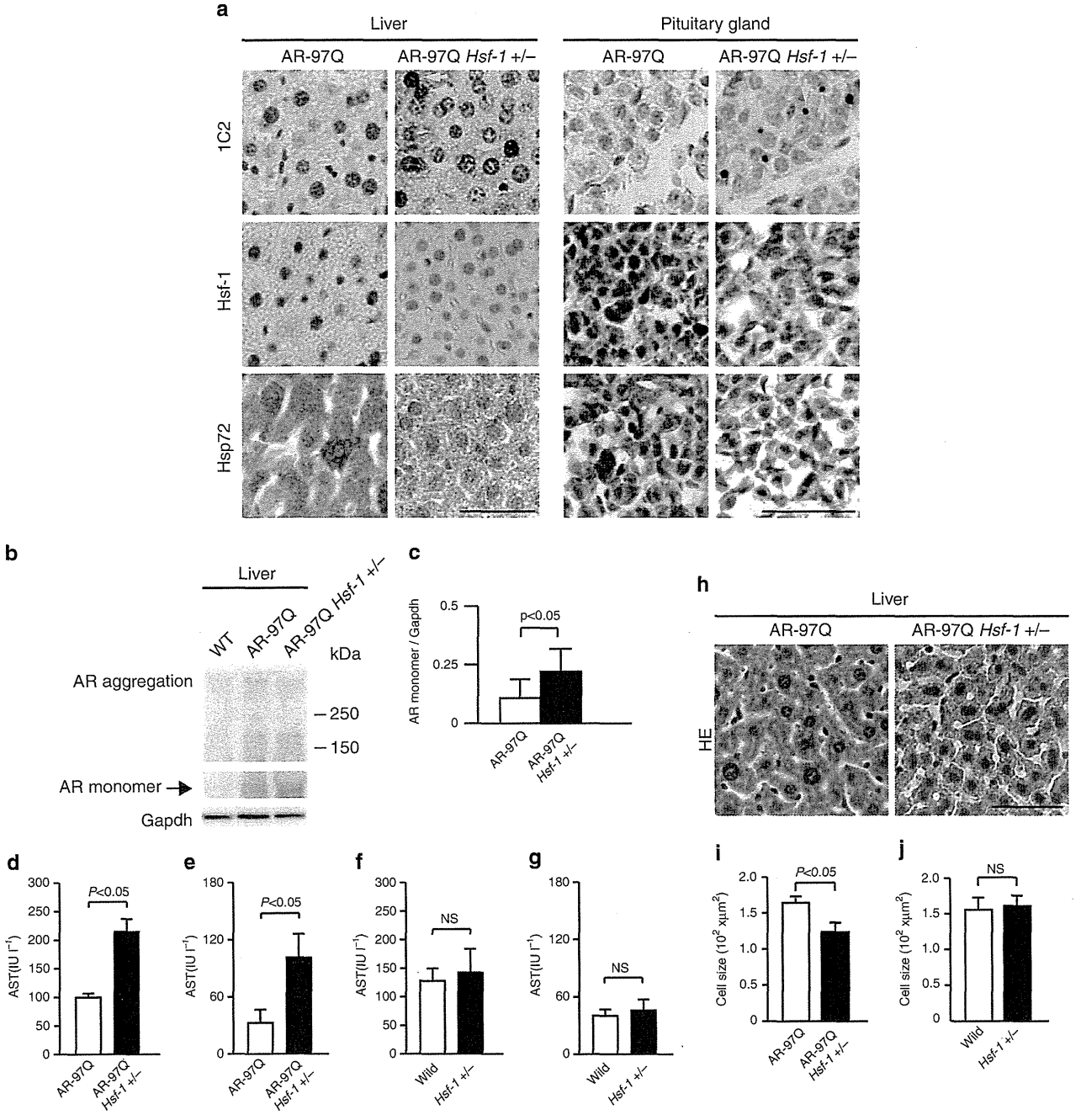

Figure 2 | Pathogenic AR accumulates in the liver and pituitary gland of heterozygous *Hsf-1*-knockout AR-97Q mice. (**a**) Immunohistochemistry of AR-97Q and *Hsf-1*-knockout AR-97Q mice using anti-Hsf-1, anti-Hsp72 and anti-polyglutamine (1C2) antibodies (13 weeks old). The *Hsf-1*-knockout AR-97Q mice showed the nuclear accumulation of pathogenic AR (yellow arrows) and decreased levels of Hsf-1 and Hsp72, an inducible form of Hsp70, in the liver and pituitary gland. (**b**) Immunoblotting for AR in wild-type, AR-97Q and *Hsf-1*-knockout AR-97Q mice (13 weeks old). (**c**) Quantification of immunoblotting revealed that the expression levels of AR monomer were upregulated in the liver of heterozygous *Hsf-1*-knockout AR-97Q mice. Unpaired *t*-test, $n=3$. (**d**–**g**) Blood tests revealed that the liver enzyme levels, including aspartate aminotransferase (AST) (**d**) and alanine aminotransferase (ALT) (**e**), were elevated in heterozygous *Hsf-1*-knockout AR-97Q mice compared with AR-97Q mice (13 weeks old). There were no significant differences in the levels of AST (**f**) and ALT (**g**) between wild-type and heterozygous *Hsf-1*-knockout mice (13 weeks old). (**h**) Haematoxylin–eosin staining of the liver of heterozygous *Hsf-1*-knockout and genetically unmodified AR-97Q mice (13 weeks old). (**i**) Quantitative analysis showed that the size of hepatocytes was reduced in heterozygous *Hsf-1*-knockout AR-97Q mice compared with AR-97Q mice. (**j**) Depletion of *Hsf-1* did not alter the size of hepatocytes in wild-type mice. Unpaired *t*-test ($n=4$) (**d**–**g**). More than 1,000 cells from three livers were analysed in each group, unpaired *t*-test. (**i**,**j**). Error bars indicate s.e.m. (**c**–**g**,**i**,**j**). Scale bars, 50 μm (**a**,**h**). NS, not significant.

through Hsp70 downregulation (Fig. 3a and Supplementary Fig. S4a). Quantitative analysis of the change in the relationship between the Hsf-1 expression levels and the frequency of 1C2-positive cells confirmed that the accumulation of pathogenic AR was significantly increased by the heterozygous depletion of Hsf-1 (Fig. 3b–e). Although pathogenic AR mainly

accumulated in the fifth and sixth layers of the cerebral motor cortex in the AR-97Q mice, where the expression levels of Hsf-1 are relatively lower than in the other layers, the distribution of pathogenic AR accumulation was expanded to the second and third layers in the heterozygous *Hsf-1*-knockout AR-97Q mice (Fig. 3f). The heterozygous knockout of *Hsf-1* also altered the distribution and frequency of pathogenic AR accumulation in neuronal and non-neuronal tissues in the AR-97Q mice (Supplementary Fig. S4b and Supplementary Table S1). To verify the impact of *Hsf-1* depletion upon the pathogenic AR aggregations, we next analysed immunoblots of the spinal cord, cerebral cortex, striatum and cerebellum using an anti-AR antibody. The findings showed that the amount of smearing AR protein, which corresponds to the toxic oligomers, was increased by the heterozygous depletion of *Hsf-1* in each part of the CNS of the AR-97Q mice (Fig. 3g–i). These findings suggest that Hsf-1 expression levels influence the degree of pathogenic AR accumulation in the SBMA mouse model.

***Hsf-1* depletion aggravates neurodegeneration in SBMA mice.** To examine whether the decreased expression levels of Hsf-1 leads to increased motor neuronal damage in the SBMA mouse model, we analysed the effects of *Hsf-1* depletion on the neurological and histopathological phenotypes of AR-97Q mice. The results demonstrated that muscle atrophy was enhanced in the *Hsf-1*-knockout AR-97Q mice compared with the genetically unmodified AR-97Q mice (Fig. 4a and Supplementary Movie 1). Footprint analysis showed that the stride length was shortened and the paws were dragged in the heterozygous *Hsf-1*-knockout AR-97Q mice (Fig. 4b,c). The heterozygous knockout of *Hsf-1* in AR-97Q mice also shortened their lifespan and decreased their body weight, and also exacerbated muscle weakness, as measured using grip power and the rotarod task (Fig. 4d–g). To exclude nonspecific effects of *Hsf-1* depletion on the motor phenotypes of wild-type mice, we investigated the lifespan and motor function of heterozygous *Hsf-1*-knockout wild-type mice (Supplementary Fig. S5a–d). The results showed that the heterozygous knockout of *Hsf-1* had no influence on the lifespan, body weight or motor function of wild-type mice, suggesting that the deleterious effects of *Hsf-1* depletion are disease-specific phenomena.

To investigate the neuropathological changes underlying the phenotypic aggravation and the increase of pathogenic 1C2-positive neuronal cells, we performed immunohistochemistry on the spinal anterior horn, cerebral cortex, striatum and cerebellum of heterozygous *Hsf-1*-knockout and genetically unmodified AR-97Q mice using antibodies against choline acetyl transferase (ChAT), NeuN and calbindin. The results showed that neurons in each part of the CNS were atrophied in the *Hsf-1*-knockout AR-97Q mice (Fig. 5a–h). Western blot analysis confirmed the decreased levels of ChAT, a functional marker of spinal motor neurons, in the heterozygous *Hsf-1*-knockout AR-97Q mice (Fig. 5i,j).

To analyse the effects of *Hsf-1* depletion on the denervation at neuromuscular junctions (NMJs) of AR-97Q mice, we performed immunofluorescent staining of NMJs using α-bungarotoxin together with antibodies against synaptophysin and phospho neurofilament (Fig. 5k). Quantitative analysis showed that the frequency of denervation at NMJ is increased in the heterozygous *Hsf-1*-knockout SBMA mice compared with the AR-97Q mice (Fig. 5l). In addition, immunohistochemistry and immunoblot analysis using an antibody against glial fibrillary acid protein (GFAP) showed increased immunoreactivity in the anterior horn of the spinal cord of the heterozygous *Hsf-1*-knockout SBMA mice compared with AR-97Q mice, indicating that motor neuron degeneration was enhanced by the partial depletion of *Hsf-1* (Fig. 5m–p). Furthermore, haematoxylin and eosin staining demonstrated that skeletal muscle fibres were atrophied in the heterozygous *Hsf-1*-knockout AR-97Q mice compared with the genetically unmodified AR-97Q mice, suggesting the aggravation of neurogenic amyotrophy (Supplementary Fig. S6a,b).

Tissue-specific regulation of Hsps in SBMA mice. To confirm that the heterozygous knockout of *Hsf-1* leads to the downregulation of Hsps, we performed immunoblotting on several tissues from each mouse group. We found that the degree of Hsf-1 downregulation differed in a tissue-specific manner in the heterozygous *Hsf-1*-knockout SBMA mice. For example, the protein levels of Hsf-1 were significantly decreased by the heterozygous knockout of *Hsf-1* in the spinal cord, liver and skeletal muscle (Fig. 6a–d). Conversely, the expression levels of Hsf-1 were not changed in the testis of the heterozygous *Hsf-1*-knockout AR-97Q mice compared with the AR-97Q mice (Fig. 6a,e). In accordance with these findings, Hsp72, the inducible form of Hsp70, was downregulated in the spinal cord and liver, but not in the testis, of the heterozygous *Hsf-1*-knockout AR-97Q mice (Fig. 6a–c,e). Moreover, Hsp105 was also significantly downregulated in the spinal cord and liver of the heterozygous *Hsf-1*-knockout mice (Fig. 6a–c). However, the expression levels of Hsps within skeletal muscle were not changed by *Hsf-1* depletion (Fig. 6a,d). Similar findings were observed in the heterozygous *Hsf-1*-knockout wild-type mice compared with wild-type mice (Supplementary Fig. S7a–d). To confirm that the downregulation of Hsp72 following *Hsf-1* depletion was via the decrease of messenger RNA levels, we analysed the mRNA expression levels of *Hsp70A1*, the gene encoding Hsp72, in the spinal cord, liver and skeletal muscle. The results showed that the mRNA levels of *Hsp70A1* were decreased in the spinal cord and liver of the heterozygous *Hsf-1*-knockout AR-97Q mice, in agreement with the immunoblotting findings (Fig. 6f,g). In contrast, the heterozygous knockout of *Hsf-1* did not alter the mRNA levels of *Hsp70A1* in skeletal muscle (Fig. 6h). There were no detectable changes in the expression levels of Hsp40 and Hsp90 in all the tissues examined from heterozygous Hsf-1-knockout AR-97Q mice (Fig. 6a–e). These findings are compatible with the change in the distribution of pathogenic AR accumulation, and indicate that the induction of Hsp70 is dependent on the expression levels of Hsf-1 in the spinal cord and liver, but not in the skeletal muscle, of the SBMA model mice.

To elucidate the molecular machinery underlying the Hsf-1-independent regulation of Hsp70 expression in the skeletal muscle of AR-97Q mice, we investigated the expression levels of several major transcription factors, such as Nfya, Tbp, p53 and Sp1, which also regulate the expression of Hsp70 (refs 18,19, 35–37). The results showed that Nfya and Sp1, but not Tbp nor p53, were upregulated in the skeletal muscle of AR-97Q mice compared with wild-type mice (Fig. 7a). This upregulation was further enhanced by the partial depletion of *Hsf-1* (Fig.7a–c). In contrast to the skeletal muscle, neither Nfya nor Sp1 were upregulated by *Hsf-1* depletion in the spinal cord or liver of AR-97Q mice (Fig. 7d,e). Immunohistochemical analysis showed an increase in the levels of nuclear Nfya and Sp1 in the skeletal muscle of AR-97Q mice, which was further intensified by the heterozygous knockout of *Hsf-1* (Fig. 7f–h). These findings suggest that proteins such as Nfya and Sp1 appear to regulate the expression of Hsp70 and this probably underlies the observation that pathogenic AR accumulation was not increased in the skeletal muscle of the *Hsf-1*-depleted AR-97Q mice.

To investigate the effects of Hsf-1 on the pathogenic AR aggregations in the skeletal muscle, we analysed immunoblots of

the tissue using an anti-AR antibody. The results showed that the amount of oligomers or monomer of pathogenic AR was not increased by the heterozygous depletion of *Hsf-1* in the skeletal muscle of AR-97Q mice (Fig. 7i,j). In agreement with these immunoblot analyses, immunohistochemistry demonstrated no significant difference in the number of 1C2-positive cells

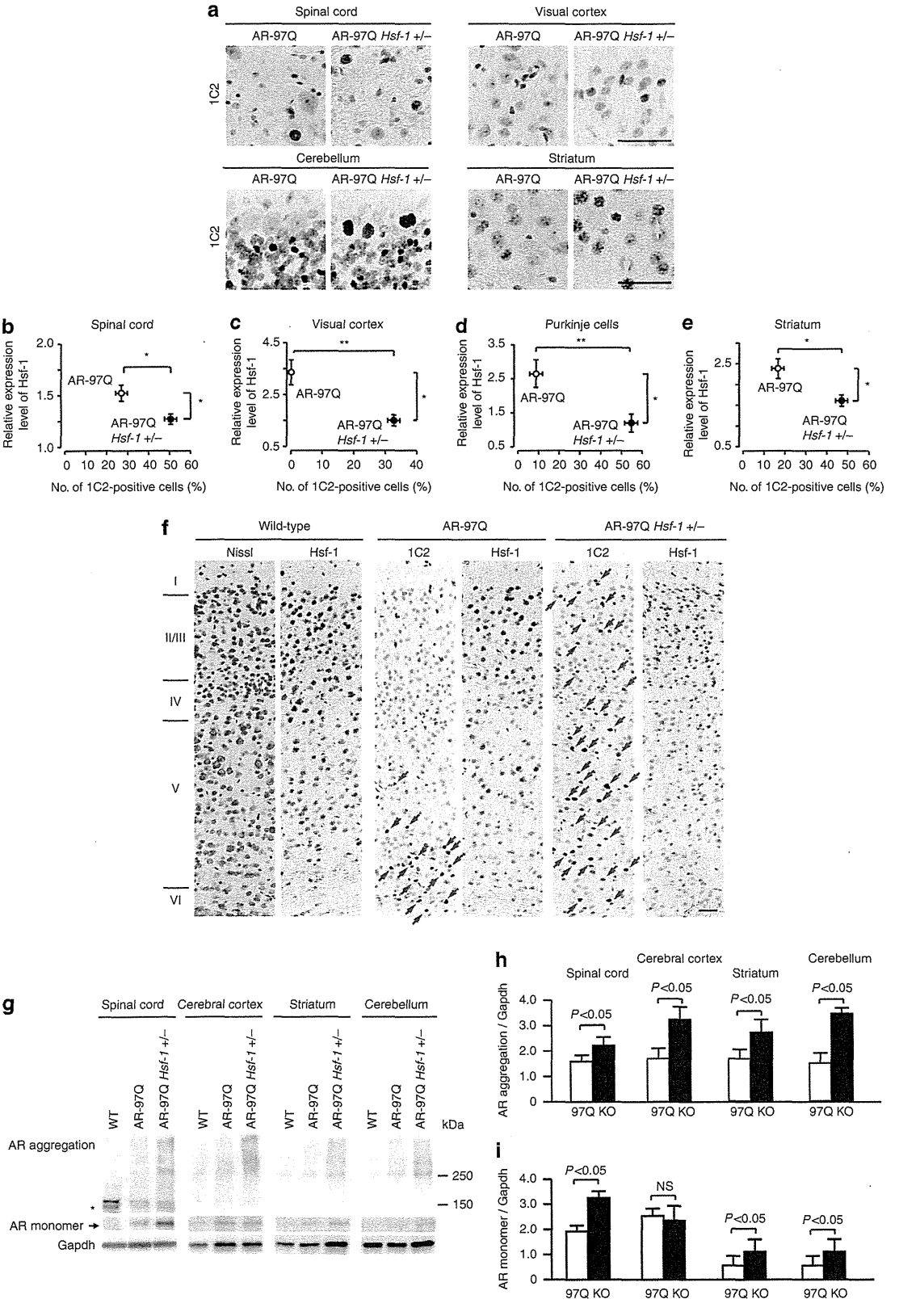

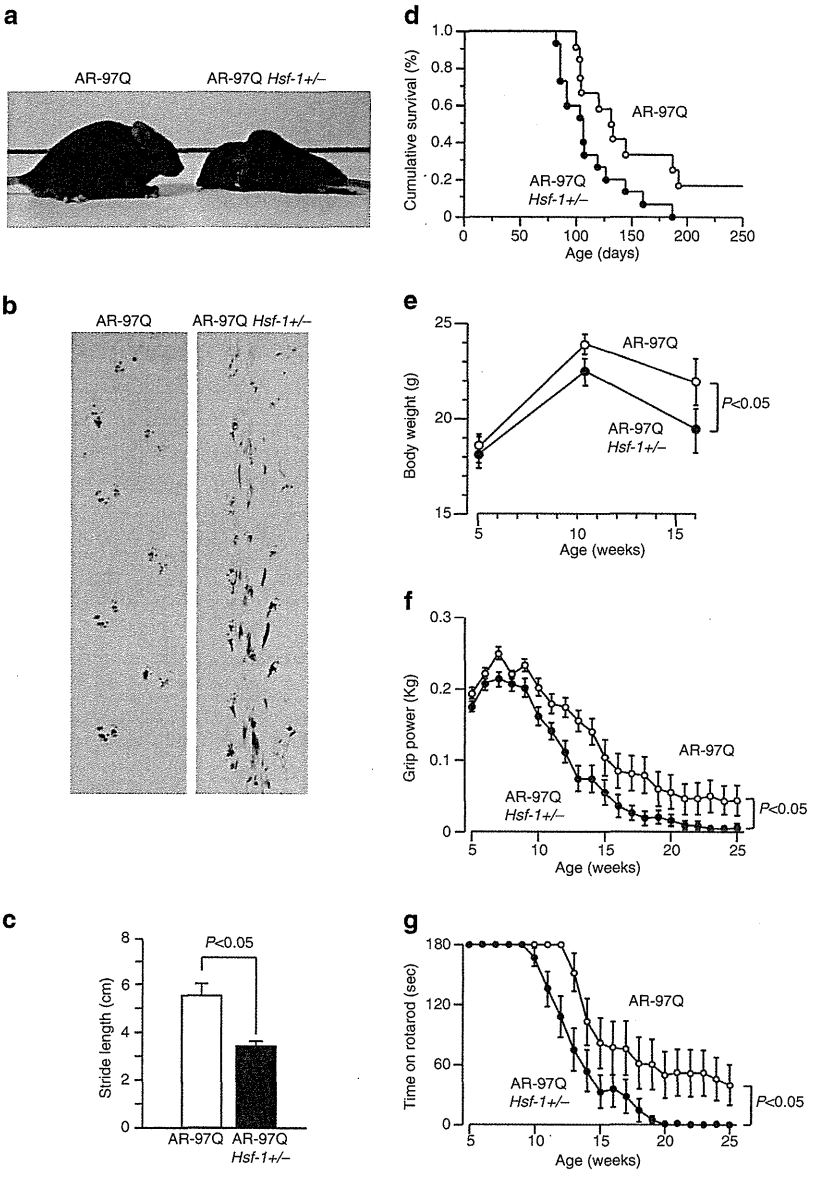

Figure 4 | Heterozygous *Hsf-1*-knockout AR-97Q mice have more severe muscle atrophy than AR-97Q mice. (**a**) Muscle atrophy is enhanced in the *Hsf-1*-knockout AR-97Q mice compared with the AR-97Q mice (10 weeks old). (**b**) Footprints of 13-week-old AR-97Q and *Hsf-1*-knockout AR-97Q mice. The front paws are shown in red, while the hind paws are shown in blue. (**c**) Quantification of the footprints revealed that the stride length was significantly shortened in the heterozygous *Hsf-1*-knockout AR-97Q mouse (13 weeks old). Unpaired *t*-test ($n=3$). Cumulative survival (**d**), body weight (**e**), grip power (**f**) and Rotarod task (**g**) of AR-97Q and *Hsf-1*-knockout AR-97Q mice. There were significant differences in all parameters between the AR-97Q ($n=12$) and heterozygous *Hsf-1*-knockout AR-97Q ($n=15$) mice by unpaired *t*-test: $P<0.05$ (**d**); $P<0.05$ at 16 weeks (**e**); $P<0.05$ at 25 weeks (**f**); and $P<0.05$ at 25 weeks (**g**). Error bars indicate s.e.m. (**c**–**g**).

Figure 3 | Augmentation of pathogenic AR accumulation in the CNS of *Hsf-1*-knockout AR-97Q mice. (**a**) Immunohistochemistry for 1C2, Hsf-1 and Hsp72 in AR-97Q and *Hsf-1*-knockout AR-97Q mice (13 weeks old). Pathogenic AR (yellow arrows) accumulated in the cerebral visual cortex of heterozygous *Hsf-1*-knockout SBMA mice where the accumulation of pathogenic AR was not observed in the AR-97Q mice. (**b**–**e**) The change in the relationship between the expression levels of Hsf-1 and the frequency of 1C2-positive neurons in the spinal anterior horn (**b**), cerebral visual cortex (**c**), Purkinje cells of the cerebellum (**d**) and striatum (**e**). (**f**) Immunohistochemistry for Hsf-1 and 1C2 in the cerebral motor cortex of AR-97Q and *Hsf-1*-knockout AR-97Q mice (13 weeks old). In AR-97Q mice, 1C2-positive cells were observed in the fifth layer of the cerebral motor cortex, where the expression levels of Hsf-1 were relatively lower than in the other layers. The distribution of pathogenic AR accumulation (red arrows) was expanded to the second and third layers of the cerebral motor cortex in heterozygous *Hsf-1*-knockout AR-97Q mice. (**g**) Immunoblotting for AR in wild-type, AR-97Q and *Hsf-1*-knockout AR-97Q mice (13 weeks old). Pathogenic AR oligomers are indicated by a smear from the top of the gel. *Nonspecific bands. (**h**) Quantitative analysis of immunoblots using densitometry indicated that the expression levels of abnormal AR protein complexes in the spinal cord, cerebral cortex, striatum and cerebellum were upregulated in heterozygous *Hsf-1*-knockout AR-97Q mice compared with AR-97Q mice. (**i**) Quantification of immunoblotting revealed that the expression levels of AR monomer were upregulated in the spinal cord, striatum and cerebellum of heterozygous *Hsf-1*-knockout AR-97Q mice. *$P<0.05$, **$P<0.01$ by unpaired *t*-test. More than 500 neurons from three brains were analysed in each group (**b**–**e**). Unpaired *t*-test ($n=3$) (**h**,**i**). Error bars indicate s.e.m. (**b**–**e**,**h**,**i**). Scale bars, 50 μm (**a**). NS, not significant.

in the skeletal muscle between the heterozygous *Hsf-1*-knockout and genetically unmodified AR-97Q mice (Supplementary Fig. S8a,b).

Overexpression of Hsf-1 suppresses AR accumulation. To investigate whether Hsf-1 exerts neuroprotection in the mouse model of SBMA, we administered a lentiviral vector expressing

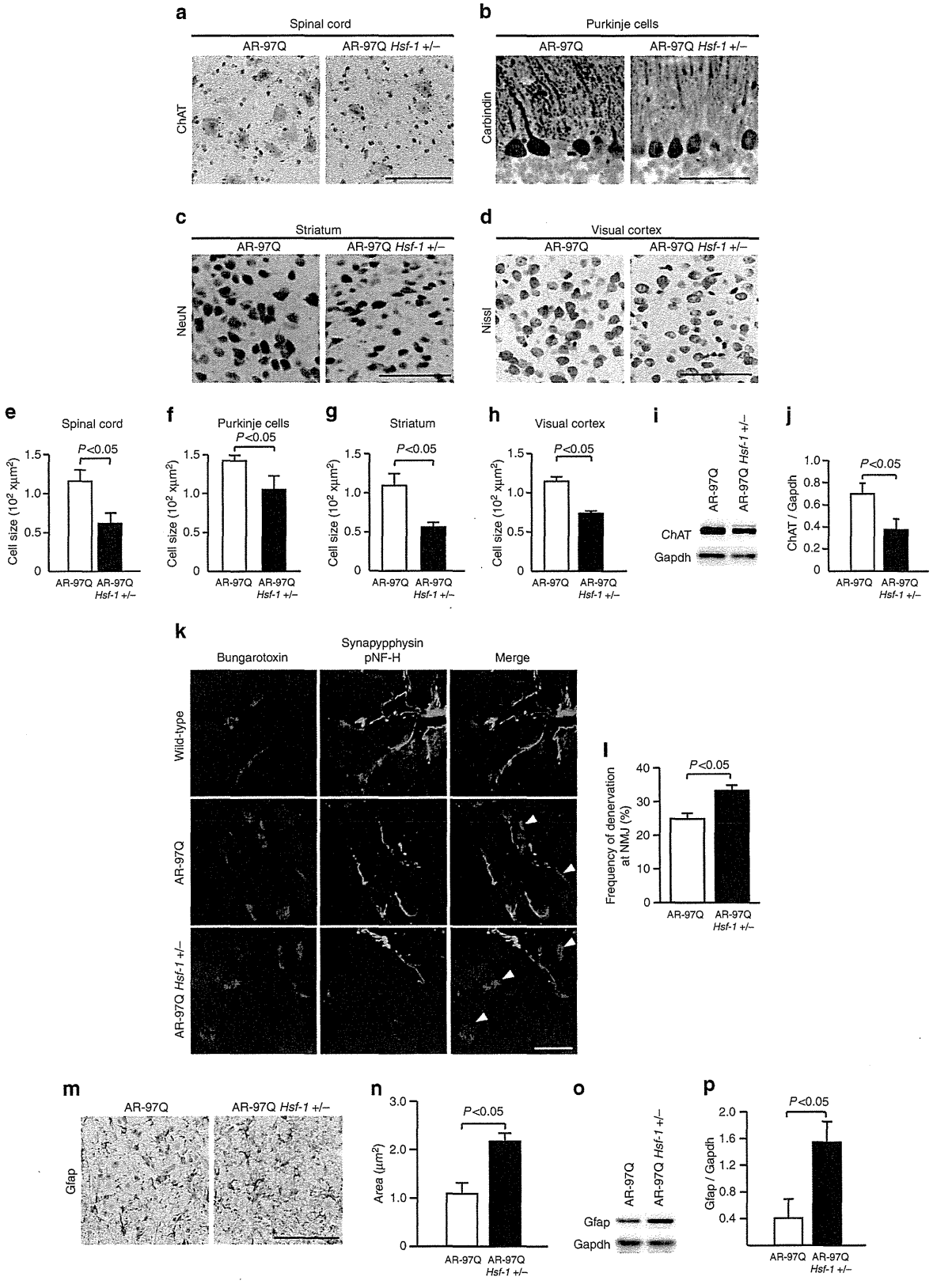

green fluorescent protein (GFP) with or without human HSF-1 into the motor cortex and striatum of the AR-97Q mice (Fig. 8a,f), as previous reports showed that no line of transgenic mice of HSF-1 demonstrates an increased expression level of this protein in the brain[38]. We performed stereotaxic injection of the lentiviral vector into the motor cortex or striatum of 8-week-old SBMA mice. Three weeks after the surgery, neuronal size and frequency of abnormal AR accumulation were examined. In both the motor cortex and striatum, the frequency of pathogenic AR accumulation around the lentiviral vector-injected area where HSF-1 was highly expressed was decreased in comparison with that in the contralateral side without treatment (Fig. 8b,g). In addition, the neuron sizes of the motor cortex and striatum were significantly increased by the *HSF-1* injecteion (Fig. 8b,g). Quantitative analyses confirmed these findings, whereas the lentiviral delivery of GFP without HSF-1 failed to show any neuroprotective effects (Fig. 8c–e,h–j and Supplementary Fig. S9a–j). These results indicated that HSF-1 overexpression attenuated the accumulation of pathogenic AR and eventual neurodegeneration in the brain of the SBMA mice.

In summary, we showed that the expression level of Hsf-1 influences the nuclear accumulation of pathogenic AR, and that the depletion of this transcription factor leads to the expanded distribution of pathological lesions and phenotypic exacerbation in the SBMA mouse model. However, these phenomena were not observed in skeletal muscle, where alternative regulators of Hsps, such as Nfya and Sp1, were upregulated. In addition, exogenous overexpression of HSF-1 using a lentivirus vector protected the neurons within the susceptible lesions of SBMA mice. Our results suggest that Hsf-1 contributes to the pathological lesion selectivity in SBMA, and that the tissue-specific regulation of Hsps should be taken into account for the development of therapies that induce the expression of molecular chaperones.

Discussion

In the present study, the heterozygous knockout of *Hsf-1* substantially augmented the nuclear accumulation of pathogenic AR in the CNS, suppressed the intraneuronal expression of Hsp70, diminished the size of affected neurons and exacerbated the neurological symptoms in a mouse model of SBMA. By contrast, the lentiviral delivery of HSF-1 attenuated pathogenic AR accumulation and neuronal atrophy in the brain of the SBMA mice. Hsps, particularly Hsp70, have a protective role in neurodegeneration by preventing the accumulation of abnormal proteins[4,39–43]. However, the role of Hsf-1 in the induction of Hsps is controversial in experiments using cellular models of polyglutamine diseases[18,19,38,44]. The results of the present study demonstrate that the expression of Hsp70, but not Hsp40, is regulated by Hsf-1 in various neurons including spinal motor neurons in the SBMA mouse model. As for the neuroprotective properties of Hsf-1 against cellular stresses, several studies showed that the overexpression of Hsf-1 suppresses the toxicity of polyglutamine-expanded proteins in cultured cells and rodents[38,44]. The present study also demonstrated the neuroprotective effects of the exogenous HSF-1 in the CNS of SBMA model mice. By contrast, the depletion of *Hsf-1* shortens the lifespan of a mouse model of HD, although the associated histopathological and biochemical alterations were not thoroughly examined[33]. Taken together, our findings indicate that the Hsf-1–Hsp70 pathway exerts neuroprotective effects via the suppression of pathogenic protein accumulation in the pathogenesis of polyglutamine-induced neurodegeneration.

The most intriguing finding of the present study is that the heterozygous depletion of *Hsf-1* altered the histopathological distribution of pathogenic AR accumulation in the AR-97Q mice, indicating a role for Hsf-1 in the selectivity of the pathogenic lesions in SBMA. The selective damage of specific subgroups of neuronal and non-neuronal cells, despite the ubiquitous expression of the causative protein, is a characteristic of neurodegenerative diseases, although the molecular mechanisms underlying this phenomenon remain unclear[23]. In patients with SBMA, the accumulation of pathogenic AR in each tissue corresponds to their clinical symptoms and findings, for example, lower motor neurons for muscle weakness and atrophy, and the pancreas for diabetes. Nevertheless, the distribution of pathogenic AR accumulation is not equivalent to the expression pattern of normal AR[20,32]. Furthermore, the accumulation of pathogenic AR is observed in specific tissues of the AR-97Q mice, although the expression of the transgene, which was regulated by a potent chicken-β-actin promoter, was also detected in tissues that showed no histopathological abnormalities[25,45]. These findings suggest that factors other than the transcription of mutant *AR* may contribute to the tissue-specific accumulation of the causative protein. In the present study, the heterozygous knockout of *Hsf-1* induced pathogenic AR accumulation in the cerebral visual cortex, liver and pituitary gland, which were not affected in genetically unmodified AR-97Q mice. In addition, the reduction of Hsf-1 expression in hepatocytes resulted in the exacerbation of liver dysfunction and cellular atrophy in the SBMA mouse model. Given that the defect of protein turnover leads to cellular atrophy[46], the impairment of protein quality control due to pathological AR accumulation induced by *Hsf-1* depletion may underlie the hepatocyte atrophy[47]. These findings indicate that endogenous Hsf-1 can clear certain lesions, such as in the cerebral visual cortex, liver and pituitary gland, of pathogenic AR accumulation and that the expression levels of Hsf-1 in each tissue, at least partially, influence the pathogenic lesion selectivity of SBMA.

Figure 5 | Histopathological change in the CNS of *Hsf-1*-knockout AR-97Q mice. (**a**–**d**) Histopathological analyses of AR-97Q and *Hsf-1*-knockout AR-97Q mice (13 weeks old). Immunohistochemistry for ChAT in the anterior horn of the spinal cord (**a**). Immunohistochemistry for calbindin in Purkinje cells (**b**). Immunohistochemistry for NeuN in the striatum (**c**). Nissl staining of the cerebral cortex (**d**). (**e**–**h**) Quantitative analysis of the size of neurons revealed that the neurons in each part of the CNS became atrophied in the *Hsf-1*-knockout AR-97Q mice compared with the AR-97Q mice. (**i**) Immunoblotting for ChAT in the spinal cord of AR-97Q and *Hsf-1*-knockout AR-97Q mice (13 weeks old). (**j**) Quantitative analysis of the signal intensity of the ChAT-immunoreactive bands. (**k**) Immunofluorescent staining of NMJs in 13-week-old AR-97Q and heterozygous *Hsf-1*-knockout AR-97Q mice (red, bungarotoxin; green, synaptophysin and phopsho-neurofilament H).The terminal of motor axons (green) are merged with virtually all the acetylcholine receptors labelled by bungarotoxin (red) in wild-type mice, indicating that NMJs are fully innervated. By contrast, some NMJs of AR-97Q mice lack synaptophysin and phopsho-neurofilament H staining owing to denervation (arrowheads), and this phenomenon was further enhanced by *Hsf-1* depletion. (**l**) The frequency of denervation at NMJ is significantly increased in heterozygous *Hsf-1*-knockout AR-97Q mice. (**m**) Immunohistochemistry for Gfap in the anterior horn of the spinal cord. (**n**) Quantitative analysis of anti-Gfap immunoreactivity. (**o**) Immunoblotting for Gfap in the spinal cord of AR-97Q and *Hsf-1*-knockout AR-97Q mice (13 weeks old). (**p**) Quantitative analysis of the signal intensity of the Gfap-immunoreactive bands. Unpaired *t*-test. More than 500 neurons from three brains were analysed in each group (**e**–**h**), $n=3$ (**j**). Unpaired *t*-test. $n=3$ for each group (**l**), $n=5$ (**n**). Error bars indicate s.e.m. (**e**–**h**,**j**,**l**,**n**,**p**). Scale bars, 50 μm (**a**–**d**,**k**,**m**).

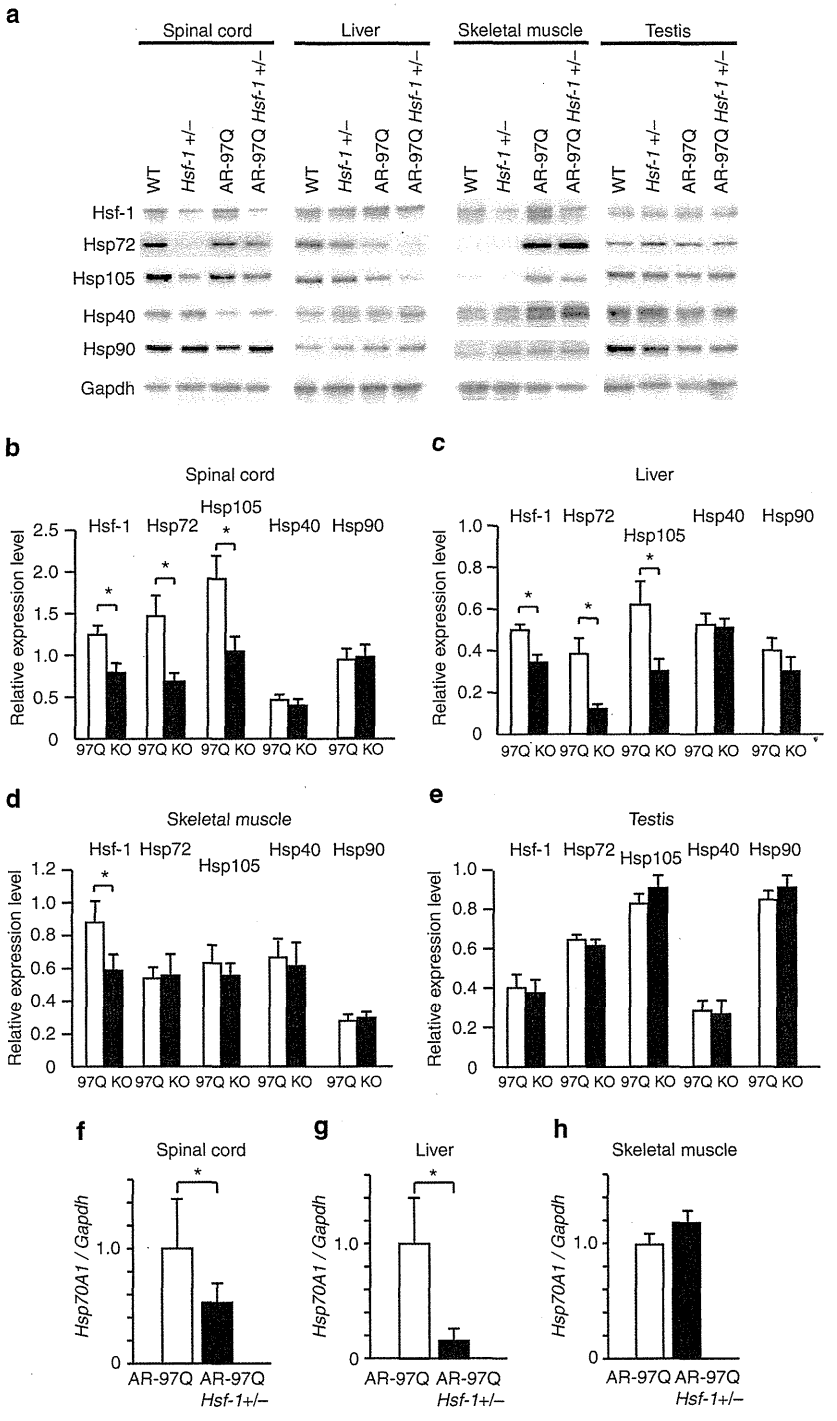

Figure 6 | Expression levels of Hsps in tissues from *Hsf-1*-knockout AR-97Q mice. (**a**) Immunoblotting for Hsf-1, Hsp72, Hsp105, Hsp40 and Hsp90 in wild-type, *Hsf-1*-knockout wild-type, AR-97Q and Hsf-1-knockout AR-97Q mice (13 weeks old). (**b**–**e**) Quantitative analysis using densitometry revealed that the expression levels of Hsp72 in the spinal cord (**b**) and liver (**c**) were downregulated in heterozygous *Hsf-1*-knockout AR-97Q mice compared with AR-97Q mice (13 weeks old). No significant alterations in the signal intensity of the Hsp-immunoreactive bands were observed in skeletal muscle (**d**) or testis (**e**). Data are shown as the ratio of the intensity of each molecule to Gapdh. (**f**–**h**) Quantification of *Hsp70A1* mRNA levels using RT-PCR in the spinal cord (**f**), liver (**g**) and skeletal muscle (**h**). $^*P<0.05$ by unpaired *t*-test ($n=7$) (**b**–**e**), and ($n=3$) (**f**–**h**). The inter-group differences were not significant, unless otherwise mentioned. Error bars indicate s.e.m. (**b**–**h**).

The results of the present study also revealed the tissue-specific regulation of Hsps by Hsf-1. Despite downregulation of Hsps in spinal cord and liver, *Hsf-1* depletion had no effect on the expression of Hsps in the testis of AR-97Q mice, presumably owing to an incomplete reduction of Hsf-1 protein levels. Furthermore, the inactivation of Hsf-1 did not decrease the expression levels of Hsps or enhance the accumulation of pathogenic AR in the skeletal muscle of SBMA mice, suggesting

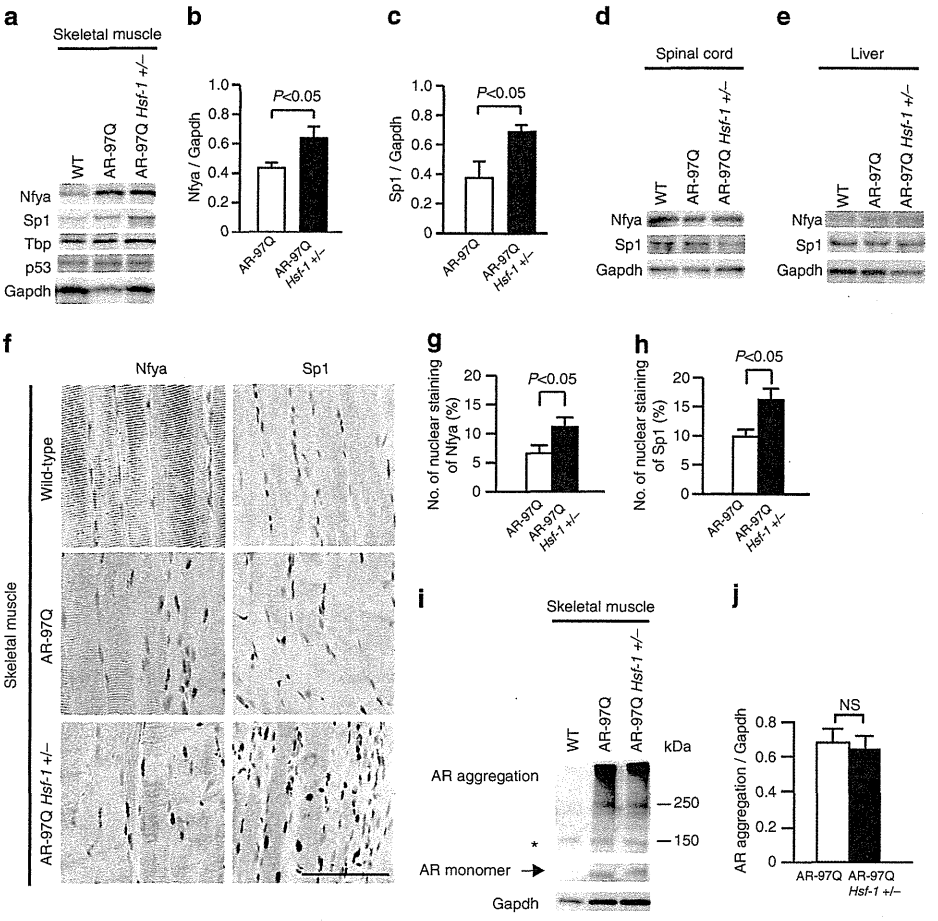

Figure 7 | Expression levels of Hsp70 inducers in skeletal muscle. (**a**) Immunoblotting for Nfya, Sp1, p53 and Tbp in wild-type, AR-97Q and heterozygous *Hsf-1*-knockout AR-97Q mice (13 weeks old). (**b**,**c**) Quantitative analysis using densitometry revealed that the expression levels of Nfya and Sp1 in skeletal muscle were upregulated in heterozygous *Hsf-1*-knockout AR-97Q mice compared with AR-97Q mice (13 weeks old). (**d**,**e**) Immunoblotting for Nfya and Sp1 in the spinal cord and liver in the mice of each group (13 weeks old). (**f**) Immunohistochemistry of skeletal muscle in wild-type, AR-97Q and *Hsf-1*-knockout AR-97Q mice using anti-Nfya and anti-Sp1 antibodies (13 weeks old). The nuclear uptake of Nfya and Sp1 was upregulated in AR-97Q mice compared with wild-type mice, and further intensified in heterozygous *Hsf-1*-knockout AR-97Q mice. (**g**,**h**) Quantification of immunohistochemistry with Nfya and Sp1 in the skeletal muscle of heterozygous *Hsf-1*-knockout AR-97Q mice compared with AR-97Q mice (13 weeks old). (**i**) Immunoblotting for AR in wild-type, AR-97Q and *Hsf-1*-knockout AR-97Q mice (13 weeks old). *Nonspecific bands. Quantitative analysis of immunoblots using densitometry indicated that the expression levels of abnormal AR aggregations in the skeletal muscle had no significant change in heterozygous *Hsf-1*-knockout AR-97Q mice compared with AR-97Q mice (**j**). Unpaired *t*-test ($n=3$). Error bars, s.e.m. (**b**,**c**,**g**,**h**,**j**). Scale bars, 50 μm (**f**). NS, not significant.

that molecules other than Hsf-1 may maintain the expression of Hsps. The upregulation of Nfya and Sp1 in the skeletal muscle of the heterozygous *Hsf-1*-knockout AR-97Q mice appears to compensate for the deleterious effects of *Hsf-1* depletion on the transcriptional regulation of Hsp70, given that these molecules are capable of inducing the expression of Hsps in certain circumstances[36,37,48]. In contrast, this compensatory mechanism does not function in the spinal cord, providing another molecular basis for the vulnerability of motor neurons in SBMA. In support of our findings, a cell-specific compensatory mechanism was shown to influence the selectivity of pathogenic lesions in a mouse model of HD[49]. As Hsf-1 is known to have diverse functions in healthy and disease conditions, such as longevity and inflammation[50,51], further study is needed to thoroughly understand the entire effects of *Hsf-1* depletion on the pathogenesis of neurodegenerative diseases. From the therapeutic point of view, the manipulation of tissue-specific regulatory systems of Hsps may be a key strategy to combat the toxicity of polyglutamine-expanded proteins.

Methods

Animals. AR-97Q mice were generated by using the pCAGGS vector and maintained as described previously[25,40]. The AR-97Q and heterozygous *Hsf-1*-knockout AR-97Q mice, as well as the heterozygous *Hsf-1*-knockout wild-type and wild-type mice used in the experiments described here, were derived by crossing heterozygous *Hsf-1*-knockout C57BL6 mice with AR-97Q mice[33]. All of the experiments were performed on male mice derived from the cross described above. The mice were genotyped by PCR on tail DNA[25,33].

Behavioural analysis. All of the tests were performed weekly, and the data were analysed prospectively as described in Supplementary Methods. All of the animal experiments were performed in accordance with the National Institutes of Health Guide for the Care and Use of Laboratory Animals and under the approval of the Nagoya University Animal Experiment Committee.

Autopsy specimens. Autopsy specimens of the CNS, including the spinal cord, cerebrum and cerebellum, and non-neuronal tissues, such as the pancreas, spleen and colon, were obtained from three genetically confirmed SBMA patients (52, 77 and 78 years old) and three control subjects (58, 64 and 70 years old). Representative sections are shown in Supplementary Fig. S2. The collection of tissues and their use for this study were approved by the Ethics Committee of Nagoya University Graduate School of Medicine.

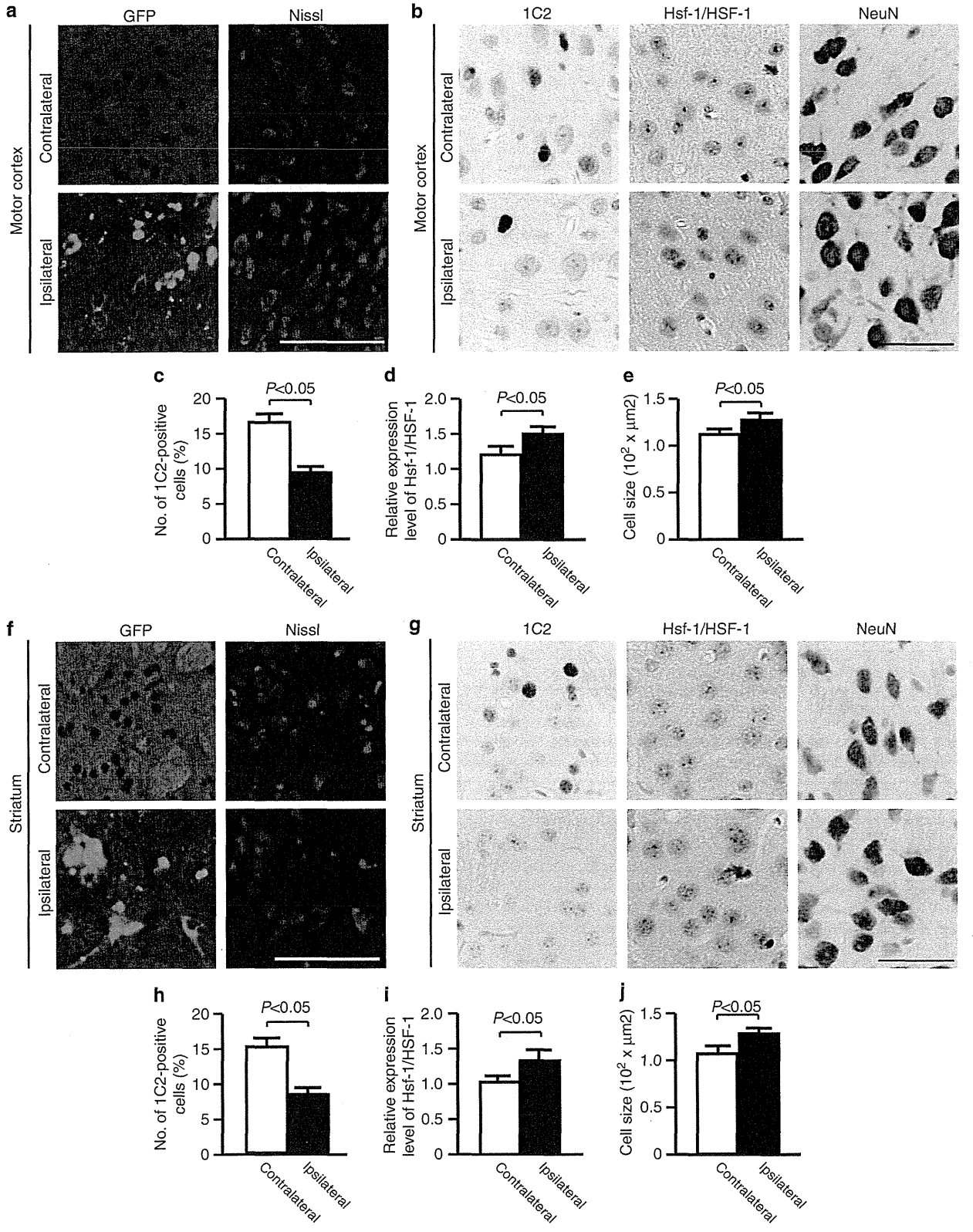

Figure 8 | HSF-1 alleviates neuronal atrophy in the motor cortex and striatum of AR-97Q mice. (**a**,**f**) Expression of transgenes in the motor cortex (**a**) and striatum (**f**) of the AR-97Q mice 3 weeks after injection. (**b**,**g**) Immunohistochemistry for Hsf-1/HSF-1, 1C2 and NeuN in the motor cortex and striatum of AR-97Q mice. The regions injected with lentiviral vector expressing hHSF-1 were compared with the contralateral side of the same mouse (13 weeks old). (**c**–**e**, **h**–**j**) Quantitative analyses of the frequency of 1C2-positive cells (**c**,**h**), relative expression level of Hsf-1/HSF-1 (**d**,**i**) and cell size of neuronal cells (**e**,**j**) confirmed the neuroprotection by the lentiviral delivery of HSF-1 into the motor cortex and striatum of AR-97Q mice. Unpaired *t*-test. More than 300 neurons from three brains were analysed in each group (**c**–**e**,**h**–**j**). Error bars indicate s.e.m. (**c**–**e**,**h**–**j**). Scale bars, 100 µm (**a**,**f**) and 50 µm (**b**,**g**).